Insights into skull evolution in fossorial snakes, as revealed by the cranial morphology of *Atractaspis irregularis* (Serpentes: Colubroidea)

Catherine R. C. Strong[a], Alessandro Palci[b,c], and Michael W. Caldwell[a,d]

[a]*Department of Biological Sciences, University of Alberta, Edmonton, Canada, T6G 2E9;* [b]*Earth Sciences Section, South Australian Museum, Adelaide, Australia, SA 5000;* [c]*College of Science and Engineering, Flinders University, Bedford Park, Australia, SA 5042;* [d]*Department of Earth and Atmospheric Sciences, University of Alberta, Edmonton, Canada, T6G 2E9*

For Peer Review Only

Abstract

Comparative osteological analyses of extant organisms provide key insight into major evolutionary transitions and phylogenetic hypotheses. This is especially true for snakes, given their unique morphology relative to other squamates and the persistent controversy regarding their evolutionary origins. However, the osteology of several major snake groups remains undescribed, thus hindering efforts to accurately reconstruct the phylogeny of snakes. One such group is the Atractaspididae, a family of fossorial colubroids. We herein present the first detailed description of the atractaspidid skull, based on fully segmented micro-computed tomography (micro-CT) scans of *Atractaspis irregularis*. The skull of *Atractaspis* presents a highly unique morphology influenced by both fossoriality and paedomorphosis. This paedomorphosis is especially evident in the jaws, palate, and suspensorium, the major elements associated with macrostomy (large-gaped feeding in snakes). Comparison to scolecophidians—a group of blind, fossorial, miniaturized snakes—in turn sheds light on current hypotheses of snake phylogeny. Features of both the naso-frontal joint and the morpho-functional system related to macrostomy refute the traditional notion that scolecophidians are fundamentally different from alethinophidians (all other extant snakes). Instead, these features support the controversial hypothesis of scolecophidians as 'regressed alethinophidians,' in contrast to their traditional placement as the earliest-diverging snake lineage. We propose that *Atractaspis* and scolecophidians fall along a morphological continuum, characterized by differing degrees of paedomorphosis. Altogether, a combination of heterochrony and miniaturization provides a mechanism for the derivation of the scolecophidian skull from an ancestral fossorial alethinophidian morphotype, exemplified by the non-miniaturized and less extreme paedomorph *Atractaspis*.

For Peer Review Only

Keywords

evolutionary development — fossoriality —heterochrony — micro-CT — miniaturization — paedomorphosis — skull anatomy — snake evolution

1. Introduction

Snakes are a major vertebrate group, comprising well over 3000 species, yet many aspects of their biology and evolution remain unknown (Harrington and Reeder, 2017; Hsiang et al., 2015). Adaptations in various lineages to functionally constrained environments and habits, such as fossoriality, further complicate interpretations of anatomy and phylogenetic relationships. The genus *Atractaspis*, known commonly as the burrowing asp, is a fossorial lineage within the Colubroidea, the most deeply nested clade of extant snakes. This genus has been noted for its distinctive skull morphology and unique feeding methods, primarily the modified palatomaxillary biomechanics which allow it to envenomate prey by protruding the fang posterolaterally while the mouth is closed (Deufel and Cundall, 2003). This unique morphology has long confounded snake systematists, resulting in varied placements of *Atractaspis* as an elapid or as a viperid in early analyses (see Underwood and Kochva, 1993 for a detailed taxonomic review). More recently, *Atractaspis* has been classified as a member of either its own family, the Atractaspididae (Jackson, 2007; Kochva, 1987, 2002; Moyer and Jackson, 2011; Shine et al., 2006; Underwood and Kochva, 1993; Zaher et al., 2009; Zaher et al., 2019), or of the subfamily Atractaspidinae within the Lamprophiidae (Portillo et al., 2019; Vidal et al., 2008).

Despite this morphological novelty, osteological descriptions of *Atractaspis* and its larger group, the Atractaspididae or Atractaspidinae, are limited; most of the literature related to

For Peer Review Only

Atractaspis has focussed on the evolution of its fangs and venom apparatus (e.g., Jackson, 2007; Kochva, 1987, 2002) or on its functional morphology and feeding biomechanics (e.g., Deufel and Cundall, 2003), resulting in descriptions and illustrations in turn focussed heavily on the teeth and on skull elements related to feeding. Only one study (Underwood and Kochva, 1993) has reviewed the overall anatomy of the Atractaspididae, though this description mainly discussed the general condition of various skull elements within this family, rather than providing a detailed description of any single genus, and was further limited almost exclusively to the select cranial features included in the study's character list. The only recent morphology-based phylogeny focussing on the Atractaspididae used external morphology, rather than osteology (Moyer and Jackson, 2011), and other recent phylogenies have exclusively employed molecular data (e.g., Portillo et al., 2019; Vidal et al., 2008; Zaher et al., 2009; Zaher et al., 2019). Descriptions of recently established species of *Atractaspis* have similarly focussed on external morphology, with descriptions of osteology limited almost entirely to skull measurements (e.g., Rödel et al., 2019).

An understanding of cranial osteology is especially important in the case of *Atractaspis*, as the fossorial habits of this genus impart strong functional constraints which are key to explaining the derivation of its unique skull morphology. As a colubroid, *Atractaspis* belongs to one of the major groups of macrostomate snakes, i.e., large-gaped snakes capable of ingesting disproportionately large prey items, comprising the Colubroidea and Booidea (Scanferla, 2016). This genus therefore provides valuable insight into how fossoriality affects a complex and highly derived morpho-functional system such as macrostomy. The status of *Atractaspis* as a fossorial colubroid also provides an interesting basis for comparison to other fossorial snakes, most prominently scolecophidians. These miniaturized snakes are traditionally considered to be the

For Peer Review Only

most primitive or basal snake lineage, forming the sister group to all other extant snakes, i.e., alethinophidians (e.g., List, 1966; Miralles et al., 2018; Rieppel, 2012). However, adaptations related to miniaturization and to fossoriality render scolecophidians highly autapomorphic and complicate interpretations of morphology and evolution.

Recognizing this importance of visualizing and understanding the skull of *Atractaspis*, our study aims to use this taxon to: examine the effect of fossoriality on the colubroid skull; assess the possible presence and extent of processes such as heterochrony; and compare *Atractaspis* to other fossorial snakes, so as to gain broader insights into the evolution of groups such as scolecophidians. To accomplish this, we present herein the first thorough osteological description and illustration of any species within the Atractaspididae, based on fully segmented micro-computed tomography (micro-CT) imagery of the skull of *Atractaspis irregularis* (Reinhardt, 1843) (Figs 1–9, S1–S23). This study thus contributes to a recently growing body of anatomical research using micro-CT data to examine un- or under-described snake taxa (e.g., Chretien et al., 2019; Olori and Bell, 2012; Palci et al., 2016; Racca et al., 2020; Rieppel et al., 2009; Rieppel and Maisano, 2007; Strong et al., 2019). This research approach provides an essential foundation for constructing higher-order hypotheses of organismal evolution and phylogenetic relationships, and is particularly important for understanding complicated but evolutionarily significant structures such as the skull.

Applying this high-resolution and non-invasive imaging across a range of taxa, we examine fossoriality-influenced structures such as the naso-frontal joint, jaws, and suspensorium, as well as the potential influence of paedomorphosis on the skull evolution of fossorial snakes, namely *Atractaspis* and scolecophidians. This analysis is especially timely given recent phylogenies recovering scolecophidians as nested within Alethinophidia (Garberoglio et al.,

For Peer Review Only

2019; Palci and Caldwell, 2010), thus providing an impetus for re-evaluating assumptions surrounding scolecophidian anatomy and evolution.

2. Material and Methods

2.1. Imaging

The main specimen featured in this study is *Atractaspis irregularis* (FMNH 62204), originally scanned at the High-Resolution X-ray CT (HRXCT) Facility at the University of Texas at Austin, as part of the Squamate Tree of Life / Deep Scaly Project. The specimen was collected in Torit, Torit District, Sudan in 1949. Scanning parameters, as provided by J. Maisano and DigiMorph.org, are: 1600 views taken for each slice, with 2 samples per view; tube voltage / current, 180 kV / 0.133 mA; no X-ray prefilter; empty container wedge; image resolution, 1024 pixels; slice thickness, 2 lines, 0.0359 mm; source-to-object distance, 52 mm; interslice spacing, 0.0359 mm; field of reconstruction, 15 mm (maximum field of view, 17.02393 mm); reconstruction offset, 6900; reconstruction scale, 1400. Reconstruction of the raw HRXCT image projections involved drift- and ring-removal processing. Further information regarding the scan parameters is available in the Supporting Information (S24).

ImageJ was used to improve the contrast and brightness of the reconstructed slices. The dataset was then loaded in Dragonfly 4.0 (Object Research Systems, 2019) for visualization. The Threshold tool was used to digitally remove remaining soft tissues from the scan, leaving only the skull. The Manual Segmentation tool was used to isolate the individual elements, with these segmentations exported as surface mesh (STL) files. These surface meshes are available as 3D PDFs in the Supporting Information (Figs S1–S23). The final segmentations were described

For Peer Review Only

qualitatively in comparison to various other specimens from a range of taxa (see §2.2). Although only the bones were observed directly in FMNH 62204, soft-tissue-related features (e.g., nerve and blood vessel pathways, muscle attachments) were inferred from studies of other taxa and specimens (see below).

FMNH 62204 was used as the primary reference specimen for this study because it is openly available for visualization on DigiMorph.org. Although this specimen does exhibit minor skeletal pathologies, as described in the Supporting Information (S25), the in-text figures display the non-pathological counterpart of the affected elements whenever possible. Other *A. irregularis* individuals (see §2.2) were also examined to ensure that the osteological descriptions herein represent the true conditions of each skull element.

2.2. Comparative Specimens and Literature

Institutional abbreviations are as follows: AMNH, American Museum of Natural History, New York, USA; FMNH, Field Museum of Natural History, Chicago, USA; FRIM, Forest Research Institute Malaysia, Kuala Lumpur, Malaysia; MCZ, Museum of Comparative Zoology, Harvard University, Cambridge, USA; SAMA, South Australian Museum, Adelaide, Australia; TMM, Texas Memorial Museum of Science and History, University of Texas at Austin, Austin, USA; TNHC, Texas Natural History Collections, Texas Memorial Museum of Science and History, University of Texas at Austin, Austin, USA; UAMZ, University of Alberta Museum of Zoology, Edmonton, Canada; UMMZ, University of Michigan Museum of Zoology, Ann Arbor, USA; USNM, Smithsonian National Museum of Natural History, Washington DC, USA; ZSM, Zoologische Staatssammlung München, Munich, Germany.

For Peer Review Only

Micro-CT scans and 3D surface renderings thereof of various specimens were observed for comparative purposes over the course of this study: *Afronatrix anoscopus* (FMNH 179335); *Agkistrodon contortrix* (FMNH 166644); *Anilius scytale* (USNM 204078); *Anomalepis aspinosus* (MCZ R-14782); *Anomalepis mexicanus* (MCZ R-191201); *Anomochilus leonardi* (FRIM 0026); *Aparallactus guentheri* (MCZ R-23363); *Aparallactus modestus* (MCZ R-182625); *Aparallactus werneri* (FMNH 250439); *Atractaspis aterrima* (AMNH R-12352); *Atractaspis bibronii* (MCZ R-190390); *Atractaspis dahomeyensis* (MCZ R-53644); *Atractaspis irregularis* (FMNH 62204); *Atractaspis irregularis irregularis* (MCZ R-48555); *Atractaspis irregularis parkeri* (MCZ R-49237); *Atractaspis microlepidota* (FMNH 58397); *Atractaspis microlepidota microlepidota* (MCZ R-53556; SAMA R36770); *Bothrops asper* (FMNH 31162); *Calabaria reinhardtii* (FMNH 117833); *Casarea dussumieri* (UMMZ 190285); *Chilabothrus striatus* (USNM 59918); *Coluber constrictor* (FMNH 135284; *Cylindrophis ruffus* (FMNH 60958); *Diadophis punctatus* (FMNH 244371); *Exiliboa placata* (FMNH 207669); *Homalopsis buccata* (FMNH 259340); *Indotyphlops braminus* (UAMZ R363); *Lampropeltis getula* (FMNH 95184); *Lamprophis fuliginosus* (FMNH 62248); *Leptotyphlops dulcis* (TNHC 60638, UAMZ R335); *Liotyphlops albirostris* (FMNH 216257); *Loxocemus bicolor* (FMNH 104800); *Naja naja* (FMNH 22468); *Natrix natrix* (FMNH 30522); *Thamnophis radix* (UAMZ R636), *Typhlophis squamosus* (USNM 289090, MCZ R-145403); *Typhlops jamaicensis* (USNM 12378); *Uropeltis melanogaster* (FMNH 167048); *Uropeltis woodmasoni* (TMM M-10006); *Xenopeltis unicolor* (FMNH 148900).

Identification and comparisons of soft-tissue-related structures (e.g., foramina for passage of nerves) were made by reference to the figures and descriptions in several papers, namely Maisano and Rieppel (2007), Rieppel (1979), Rieppel and Maisano (2007), Rieppel et al. (2009),

For Peer Review Only

and Underwood and Kochva (1993). Anatomical terminology in our descriptions follows these papers, as well as Strong et al. (2019). In the figures, abbreviations of elements are from Strong et al. (2019), in turn modified from Rieppel et al. (2009) and Rieppel and Maisano (2007); abbreviations of features are original, though follow the format of Chretien et al. (2019).

3. Results

We herein provide a description of each element of the skull of *Atractaspis irregularis* (Figs 1, S1–S23), grouped according to skull region (Figs 2–9). Note that the jugal (following the primary homology arguments of Palci and Caldwell, 2013) is absent in *Atractaspis irregularis*, as is typical of this genus (Deufel and Cundall, 2003; Underwood and Kochva, 1993).

Because *Atractaspis irregularis* is a fossorial colubroid, comparisons to non-fossorial (i.e., more 'typical') colubroids are essential in understanding its unique morphology and adaptations. As such, comparisons to other snake taxa are made throughout, based on direct observations of several specimens as well as figures and descriptions provided in several papers (§2.2). *Thamnophis radix* (Colubroidea: Colubridae) was used as the exemplar for a 'typical' colubroid due to the availability of fully segmented micro-CT scans for this species (see Strong et al., 2019 and associated data).

3.1. Snout

3.1.1. Premaxilla

The premaxilla is a triaxial structure consisting of the nasal process dorsally, the paired vomerine processes posteriorly, and the transverse processes laterally (Fig. 2A–H). The nasal

For Peer Review Only

process is stout and globular, rising posterodorsally from the anterior midline of the premaxilla to articulate with the anteroventral extent of the nasal (Figs 1A, 2A–E). The transverse processes form broad wings extending posterolaterally from the base of the nasal process (Fig. 2G). The anterior surface of the premaxilla bears two lateral premaxillary foramina, each of which extends at a slight posterolateral angle to exit from the posterior surface of the premaxilla (Fig. 2E–H). Another pair of premaxillary foramina is present on the ventral surface of the premaxilla, at the junction between the vomerine and transverse processes. The vomerine processes project off a broad shelf extending posteriorly from the premaxilla (Fig. 2G). They underlie the anterior processes of the septomaxillae and extend posteriorly toward—but do not contact—the premaxillary processes of the vomers (Figs 1A,C–D, 2A–B). Altogether, the premaxilla is more tightly integrated into the snout complex than is typical of colubroids (e.g., *Thamnophis radix*, *Afronatrix anoscopus*, *Agkistrodon contortrix*, *Coluber constrictor*, *Diadophis punctatus*), due largely to its increased contact with the nasal.

3.1.2. Nasal

The nasals of *Atractaspis irregularis* are elongated and broadened relative to non-fossorial colubroids (e.g., *Thamnophis radix*, *Afronatrix anoscopus*, *Coluber constrictor*, *Diadophis punctatus*, *Homalopsis buccata*, *Agkistrodon contortrix*, *Bothrops asper*), resulting in much stronger articulation with the frontal posteriorly, the septomaxilla ventrally, and the premaxilla anteriorly (Figs 1A–B, 2A–D). This elaboration and increased integration of the snout complex occurs in several other fossorial snakes (C.S., pers. obs., e.g., *Anilius scytale*, *Anomochilus leonardi*, *Leptotyphlops dulcis*, *Liotyphlops albirostris*, *Typhlophis squamosus*, *Typhlops jamaicensis*; see also Cundall and Rossman, 1993; Rieppel et al., 2009). The nasals are roughly rectangular in dorsal view, with the anterior margins of the dorsal laminae diverging

For Peer Review Only

anterolaterally to create a V-shaped notch that accommodates the nasal process of the premaxilla (Figs 1A, 2B–D,S). A small flange projects posterolaterally just anterior to the posterolateral corner of each dorsal lamina (Fig. 2S–U). The medial nasal flanges, or vertical laminae of the nasals, articulate ventrally with the septomaxillae along nearly their entire length and articulate posteriorly with the medial frontal flanges (Figs 1A–B, 2B,T–U); in contrast, the nasals of non-fossorial colubroids (e.g., *T. radix*, *A. anoscopus*, *C. constrictor*, *D. punctatus*, *A. contortrix*) typically exhibit minimal contact with the septomaxillae and minimal to no contact with the frontal (C.S., pers. obs.; Rieppel, 2007). Most of the ventral border of each medial nasal flange is thickened in association with the extensive articulation of the nasals with the septomaxillae (Fig. 2T–U).

3.1.3. Septomaxilla

Each septomaxilla bears a medial ascending lamina, forming a thin, dorsomedially-angled ridge along its medial margin (Fig. 2A–B,I,K). This lamina extends anteromedially as a thin anterior process overlying the corresponding vomerine process of the premaxilla (Figs 1C–D, 2A–B). The medial ascending lamina also projects as a long, thin posterior process which overlies the dorsomedial surface of the corresponding vomer (Figs 1C–D, 2B,I–L). The posterior terminus of this process curves laterally (Fig. 2K–L) and underlies the anteroventral corner of the corresponding medial frontal flange, where the medial frontal pillar meets the subolfactory process of the frontal (Fig. 3G), thus participating in the naso-frontal joint as is typical of colubroids (Rieppel, 2007). The septomaxilla articulates along most of its dorsal border with the ventral margin of the corresponding medial nasal flange via the medial ascending lamina (Fig. 2B), a contact which is typically much less extensive in other colubroids (e.g., *Thamnophis radix*, *Afronatrix anoscopus*, *Coluber constrictor*, *Diadophis punctatus*, *Agkistrodon contortrix*).

For Peer Review Only

The lateral ascending lamina of each septomaxilla forms a broad but thin hook which curves around the lateral midpoint of the nasal cavity (Fig. 2A–D,I–L). The posterior surface of the septomaxilla articulates with the vomer and bears a broad, dorsomedially angled cavity surrounding the anterior extent of the vomeronasal cupola (Fig. 2B,J–K).

3.1.4. Vomer

The vomer is a globular element that articulates anteriorly and dorsomedially with the septomaxilla (Fig. 2B). The vomer is largely hollow, with a rounded internal cavity that forms the majority of the vomeronasal cupola housing the vomeronasal organ (Fig. 2Q), the anteriormost extent of which is surrounded by the septomaxilla (Rieppel, 2007; Rieppel et al., 2009; Rieppel and Maisano, 2007). Anteromedially, the premaxillary processes of the vomer occur as triangular projections articulating with the posteromedial surface of the corresponding septomaxilla, ventral to the anterior extent of the vomeronasal cupola as delimited by the septomaxilla (Figs 1C–D, 2M–P). However, these processes are shorter than in other colubroids (e.g., compared to *Thamnophis radix*, *Afronatrix anoscopus*) and do not extend far enough anteriorly to contact the vomerine processes of the premaxilla (Fig. 1C–D). The fenestra vomeronasalis occurs along the anterior border of the ventral surface of the vomer, separating the premaxillary process of the vomer medially and the lateral wall of the vomer and vomeronasal cupola laterally (Fig. 2P). The palatal processes extend posteriorly as a thin, flat projection from each ventromedial corner of each vomer (Figs 1C–D, 2M–R). These processes approach, but do not contact, the choanal processes of the palatines (Fig. 1C–D).

3.2. Skull Roof

For Peer Review Only

3.2.1. Frontal

Whereas the frontal typically bears a distinct supraorbital ridge along the dorsal border of the orbit in colubroids (e.g., *Thamnophis radix*), in *Atractaspis irregularis* this ridge is absent. In non-fossorial colubroids (e.g., *T. radix*, *Agkistrodon contortrix*, *Naja naja*, *Diadophis punctatus*, *Coluber constrictor*, *Afronatrix anoscopus*), the optic foramen is a large opening bordered anteromedially by the frontal, posterolaterally by the parietal, and ventrally by the parasphenoid rostrum of the parabasisphenoid (e.g., see Strong et al., 2019:fig. 1). In contrast, expansion of the descending flange of the frontal and the parasphenoid rostrum in *A. irregularis* relative to non-fossorial colubroids results in pronounced reduction of the orbit and optic foramen (Figs 1A, 3E,H), as occurs commonly in fossorial snakes (e.g., *Leptotyphlops dulcis*, *Typhlops jamaicensis*, *Typhlophis squamosus*, *Liotyphlops albirostris*, *Anomochilus leonardi*). The optic foramen is bordered mainly by the frontal, forming a narrow canal running posteromedially along the juncture of the posteroventral processes of the frontal with the rest of the frontal (Fig. 3E,H). These posteroventral processes represent an expansion of the descending flange of the frontal and articulate with the expanded parasphenoid rostrum of the parabasisphenoid (Figs 1A, 3E–F), thus excluding the parabasisphenoid entirely from the optic foramen. The descending flanges of the frontal also bear broad articulatory surfaces ventrally where they contact the parasphenoid rostrum (Fig. 3F,H). The parietal contributes slightly to the posterolateral enclosure of the optic foramen (Fig. 1A).

Anterolaterally, the frontal bears deep facets for its articulation with the prefrontal (Fig. 3E). This suture is more extensive than in non-fossorial colubroids (e.g., *Afronatrix anoscopus*, *Coluber constrictor*, *Diadophis punctatus*, *Homalopsis buccata*, *Agkistrodon contortrix*, *Naja naja*), due mainly to elaboration and thickening of the prefrontal.

For Peer Review Only

The medial frontal pillars separate the olfactory tracts and are each fused to the corresponding subolfactory process of the frontal, forming the medial frontal flanges as is typical of caenophidians (Fig. 3G; Rieppel, 2007). These flanges are well-developed and tightly integrated with the medial nasal flanges (Figs 1B, 3A). The frontal also articulates anteroventrally with the posterior processes of the septomaxillae. This structure of the naso-frontal joint contrasts that of most other, non-fossorial colubroids, in which the main articulation between the snout and the rest of the skull typically occurs via the septomaxilla-frontal suture, with no contact between the frontal and the nasal (Rieppel, 2007).

3.2.2. Parietal

The parietal exhibits a tight sutural contact with all of the surrounding elements, except for openings where it forms the posterior border of the optic foramen (just dorsal to the anteroventral corner of the parietal) and the dorsal border of the primary anterior opening of the Vidian canal (just posterior to its anteroventral corner, along the suture with the parabasisphenoid) (Fig. 1A). The anterior border of the parietal flares laterally so as to broadly overlap the posterior border of the frontal (Fig. 3A–D). The dorsal surface of the parietal is smooth in FMNH 62204, with neither a sagittal sulcus nor a sagittal crest (Fig. 3A), though other observed *A. irregularis* individuals (*A. irregularis irregularis*, *A. irregularis parkeri*) do show a slight sagittal sulcus. The dorsal surface of the parietal bears a small foramen, likely for a pair of blood vessels (see Palci et al., 2019). This foramen is variably present in the species; for example, it can be observed in a specimen of *A. irregularis parkeri* (MCZ R-49237), but is absent in *A. irregularis irregularis* (MCZ R-48555). The internal surface of the parietal roof bears two shallow, lobate depressions, separated medially by a slight ridge that extends from the anterior border of the parietal roof and diverges near the posterior border of the parietal (Fig.

For Peer Review Only

3C). The parietal roof thickens posteromedially, resulting in a dorsoventrally deep sutural surface with the supraoccipital and the dorsal extent of the prootic.

3.3. Palatomaxillary Complex

3.3.1. Pterygoid

Typically, in 'macrostomatans' (booids and caenophidians), the pterygoid extends posteriorly beyond the level of the occipital condyle (C. S., pers obs.; Scanferla, 2016). This occurs in some *Atractaspis irregularis* individuals (FMNH 62204; Fig. 4A), but in others the pterygoid terminates at the level of the occipital condyle (MCZ R-49237, MCZ R-48555). This intraspecific variation may be related to the posterior expansion of the pterygoid that occurs throughout ontogeny in other macrostomatans (Palci et al., 2016; Scanferla, 2016; Strong et al., 2019). In comparison, non-'macrostomatan' snakes, including fossorial taxa, typically possess pterygoids which terminate anterior to the occipital condyle (e.g., *Cylindrophis ruffus*, *Anilius scytale*, *Uropeltis melanogaster*, *Uropeltis woodmasoni*, *Anomochilus leonardi*, *Typhlops jamaicensis*, *Leptotyphlops dulcis*). Unlike typical 'macrostomatans', the pterygoid of *A. irregularis* lacks teeth and is much less robust overall (Figs 4, 5A–D). This thin, elongate, edentulous morphology occurs in several other fossorial snakes (C.S., pers. obs., e.g., scolecophidians: *T. jamaicensis*, *L. dulcis*, *A. leonardi*; to a lesser extent, basal alethinophidians such as *U. melanogaster* and *U. woodmasoni*; see also Cundall and Rossman, 1993), though some fossorial taxa (e.g., *C. ruffus*, *A. scytale*) do exhibit a more robust, toothed morphology comparable to that of more derived alethinophidians.

The dorsal surface of the pterygoid is smooth, with a slight facet anteriorly where it is overlain by the posterior terminus of the ectopterygoid (Fig. 5C). A thin ledge projects laterally

For Peer Review Only

along the midpoint of the dorsal margin of the pterygoid in FMNH 62204 (Fig. 5A). This may represent a highly reduced remnant of the lateral flange of the quadrate process, a feature present and well-developed in *Aparallactus* (C.S., pers. obs.); however, as this ledge is absent in all other *Atractaspis* specimens examined, this more likely represents minor individual variation in this element. The right pterygoid of FMNH 62204 shows a pathology (healed fracture) at its posterior terminus (Fig. 4A), but its left counterpart is intact and shows the typical tapering to a gently rounded extremity that is typical of the genus (Fig. 4B,C).

The pterygoid is broadly separated from the palatine anteriorly, articulating only with the ectopterygoid (Figs 1C–D, 4). The pterygoids distinctly underlie the braincase (Fig. 4A), similar to *Typhlops jamaicensis*, several colubroids (e.g., *Thamnophis radix*, *Natrix natrix*, *Lampropeltis getula*, *Lamprophis fuliginosus*, *Diadophis punctatus*, *Coluber constrictor*, *Afronatrix anoscopus*, *Homalopsis buccata*), and, to a lesser extent, *Leptotyphlops dulcis*. This is in contrast to other fossorial taxa, in which the pterygoids are almost in dorsal contact with the braincase (e.g., *Uropeltis melanogaster*, *U. woodmasoni*, *Anomochilus leonardi*, and to a lesser extent *Cylindrophis ruffus* and *Anilius scytale*).

3.3.2. Ectopterygoid

The ectopterygoid of *Atractaspis irregularis* consists of an elongate, rod-like pterygoid process posteriorly and a medially expanded maxillary process anteriorly (Fig. 5E–F), as in other alethinophidians (e.g., *Thamnophis radix*, *Coluber constrictor*, *Diadophis punctatus*, *Homalopsis buccata*, *Lamprophis fuliginosus*, *Lampropeltis getula*, *Afronatrix anoscopus*, *Natrix natrix*). This morphology of the ectopterygoid contrasts the condition in some other fossorial taxa (e.g., *Calabaria reinhardtii*, *Liotyphlops albirostris*, *Typhlops jamaicensis*, *Anomochilus leonardi*, *Uropeltis melanogaster*, *Anilius scytale*, *Cylindrophis ruffus*), in which the ectopterygoid is

For Peer Review Only

greatly reduced. Note that this reduction of the ectopterygoid is not limited to fossorial taxa, as non-burrowing taxa such as *Chilabothrus striatus* and *Exiliboa placata* exhibit a similar modified form. The ectopterygoids of viperids such as *Agkistrodon contortrix* and *Bothrops asper* are similar in form to those of *A. irregularis*, except that they are more robust.

3.3.3. Palatine

The palatine of *Atractaspis irregularis* is highly reduced compared to other colubroids (e.g., *Thamnophis radix*, *Natrix natrix*, *Lampropeltis getula*, *Lamprophis fuliginosus*, *Diadophis punctatus*, *Coluber constrictor*, *Afronatrix anoscopus*, *Homalopsis buccata*), most notably in that it is dramatically shortened anteroposteriorly and bears a maximum of only four teeth (Figs 4, 5G–K; Berkovitz and Shellis, 2017). In comparison to other fossorial snakes, the palatine of *A. irregularis* most closely resembles the condition in *Typhlops jamaicensis* and, to a lesser extent, *Leptotyphlops dulcis*, *Anomochilus leonardi*, and *Calabaria reinhardtii*. In contrast, other fossorial snakes (e.g., *Anilius scytale*, *Cylindrophis ruffus*) typically possess a more robust palatine, though in some taxa it is edentulous (e.g., *Uropeltis melanogaster*, *U. woodmasoni*). The main body of the palatine is slightly medially concave and is roughly triangular, with its apex pointing posteriorly (Fig. 5H). Laterally, the maxillary process occurs as a short hook projecting anterolaterally from the dorsal apex of the palatine (Fig. 5G,I–K). The choanal process of the palatine is much more elongate, forming a spindly hook that curves broadly anteromedially before looping posteroventrally (Fig. 5G–K). Uniquely, even among fossorial snakes, the palatine is broadly separated from the pterygoid (Figs 1C–D, 4); this has been recognized as an autapomorphy of atractaspids, including aparallactine snakes (Deufel and Cundall, 2003).

For Peer Review Only

3.3.4. Prefrontal

The prefrontal is typically subdivided into three major components in snakes: the orbital wall, the outer wall, and the dorsal lappet (Maisano and Rieppel, 2007). However, this morphology is quite modified in *Atractaspis irregularis* due to greater integration of the prefrontal with the surrounding elements (Figs 1A–B, 4, 5L–Q). Medially, the prefrontal-frontal articulation is elaborated (Fig. 5O). The dorsal lappet of the prefrontal is robust and extends anteromedially (Fig. 5M–N,P–Q). At the junction between the dorsal lappet and orbital wall, prominent forked processes extend posteromedially (Fig. 5L,N–O,Q). Altogether these processes create a tight interlocking articulation between the prefrontal and anterolateral corner of the frontal (Figs 1A–B, 4A). The orbital wall is highly modified compared to other colubroids, as is to be expected given the reduction and extensive modification of the orbit itself; this component of the prefrontal is essentially replaced by the aforementioned forked processes (Fig. 5O). The ventral surface of the prefrontal is also modified so as to interlock with complementary processes on the dorsal surface of the maxilla (Figs 4, 5L,R–S). The lacrimal duct extends through the ventromedial corner of the prefrontal (Fig. 5O).

3.3.5. Maxilla

The maxilla is highly modified compared to other snakes. In a more 'typical' colubroid skull (e.g., *Thamnophis radix*, *Natrix natrix*, *Lampropeltis getula*, *Lamprophis fuliginosus*, *Diadophis punctatus*, *Coluber constrictor*, *Afronatrix anoscopus*), the maxilla is roughly equal in length to the dentary and bears teeth along its entire length. In contrast, the maxilla of *Atractaspis irregularis* is greatly shortened anteroposteriorly, such that it is equal in anteroposterior depth to the prefrontal (Figs 1A–B, 4, 5R–U). The maxillary teeth are also highly modified: each maxilla bears only two fang sockets, with only one fang—the functional tooth—

For Peer Review Only

being ankylosed to the maxilla (Fig. 5R–U; Deufel and Cundall, 2003; Jackson, 2007; Underwood and Kochva, 1993). Several smaller replacement teeth are present posterior to each maxilla and posterolingual to the functional teeth (four associated with the left maxilla and six with the right) (Figs 1, 4, 5R–U). The structure of the replacement teeth is consistent with developmental observations that formation of the fangs begins at the distal tip and proceeds toward the tooth base (Fig. 5R–U; Jackson, 2007). The teeth—including the replacement teeth—are hollow, i.e., are 'tubular fangs' sensu Jackson (2007), meaning that the venom groove is completely enclosed to form a channel within the tooth. A grooved opening ventrally on the tooth base marks the entrance of the venom duct into the enclosed venom channel of the tooth (Fig. 5R,U).

The anterodorsal surface of the maxilla of *Atractaspis irregularis* bears three processes which interlock with the notched ventral surface of the prefrontal (Fig. 5R–S); these likely represent a highly modified nasal or facial process. The maxilla abuts posteriorly against the anterolateral corner of the ectopterygoid (Fig. 4A–B). The superior alveolar canal pierces the maxilla mediolaterally through its anterior surface (Fig. 5R–S), marking the lateral and medial openings for the anteriorly extending V2 maxillary branch of the trigeminal nerve, as well as associated blood vessels (Evans, 2008).

3.4. Braincase

3.4.1. Parabasisphenoid

The parabasisphenoid is roughly triangular in dorsal view and consists of a rounded main body posteriorly and an anterodorsally directed rostrum anteriorly (Fig. 6B,D–F). These represent the basisphenoid and parasphenoid components of this bone, respectively. The ventral

For Peer Review Only

surface bears the basipterygoid processes on either side of the midline, extending from the centre of the main body to the junction between the basisphenoid and parasphenoid rostrum (Fig. 6E). The lateral borders of the parabasisphenoid are linear, lacking protrusions such as the clinoid processes (Fig. 6D–F; see Strong et al., 2019:fig. 6 for comparison to condition in *Thamnophis radix)*. The dorsal surface of the main body is generally smooth, with slight depressions anterior and posterior to the midpoint (Fig. 6D). The posterior of these represents a very weakly defined sella turcica (Fig. 6D). However, a distinct ossified dorsum sellae overhanging the sella turcica is absent; i.e., the dorsal crest along the posterior border of the sella turcica as seen in most other snakes (e.g., *Thamnophis*; see Strong et al., 2019:fig. 6) is low to absent in *Atractaspis irregularis* (Fig. 6D). This condition occurs in all observed specimens of *A. irregularis* (though see Sheverdyukova and Kovtun, 2020 for comments on the highly variable development and morphology of this region in other snakes).

The posterior opening of the Vidian canal is present just anterior to the point where the basioccipital, parabasisphenoid, and prootic meet (Fig. 6C). This canal transmits several blood vessels and nerves, including the internal carotid artery and palatine branch of the facial nerve (Evans, 2008). The left posterior opening of the Vidian canal is much larger than the right opening, likely due to asymmetry in the size of the arteries passing through these openings (Underwood and Kochva, 1993). The Vidian canal communicates with the inside of the braincase via the internal carotid foramina at the posterior corners of the parabasisphenoid (Fig. 6F). The primary anterior opening of the Vidian canal is present as a small foramen near the anterior extent of the parietal-parabasisphenoid suture (Fig. 6A,C–F), with the secondary anterior opening of the Vidian canal occurring as an even smaller foramen near the posterior extent of the frontal-parabasisphenoid suture, ventral to the optic foramen (Fig. 6A,C–F). Each of these

For Peer Review Only

anterior openings is preceded by a narrow groove on the dorsal surface of the parabasisphenoid (Fig. 6D,F).

The most notable feature of the parabasisphenoid is the laterally expanded parasphenoid rostrum (Fig. 6D–F). Typically, in colubroids (e.g., *Diadophis punctatus*, *Thamnophis radix*), the parasphenoid rostrum forms a thin process projecting anterodorsally from the basisphenoid portion of the parabasisphenoid (though see *Afronatrix anoscopus*, which also bears a broadened parasphenoid rostrum). In contrast, the parasphenoid rostrum in *Atractaspis irregularis* forms a broad shelf underlying the similarly expanded descending flanges of the frontal, with a longitudinal ridge on its dorsal surface that slots between the paired descending frontal flanges (Figs 3H, 6D,F). The rostrum thus articulates extensively along its entire length with the frontal, resulting in greater integration of these elements relative to non-fossorial colubroids. Elaboration of the descending flanges of the frontal causes the parasphenoid rostrum to be excluded from the border of the optic foramen (Figs 1A, 6A).

3.4.2. Basioccipital

The basioccipital articulates along broad sutures with the prootic anterodorsally, the otoccipital posterodorsally, and the parabasisphenoid anteriorly (Fig. 6A–C). The internal surface of the basioccipital forms a smooth, oval-shaped basin (Fig. 6G), whereas the ventral surface of the basioccipital is convex and roughly hexagonal (Fig. 6H). The occipital condyle is broad and forms a rounded lip protruding slightly ventrally from the posterior margin of the basioccipital (Fig. 6B–C,G–H). The basioccipital tubercles extend posterolaterally as small, wing-like processes from each lateral apex of the basioccipital (Fig. 6G–H).

3.4.3. Prootic

The prootic articulates with the supratemporal laterally, with a slight indent centrally on

For Peer Review Only

the dorsolateral surface of the prootic to accommodate this articulation (Figs 1A, 6A, 7A). Ventral to this facet, the prootic bears four large foramina on its lateral surface (Figs 6A, 7A).

The two dorsal-most foramina represent a subdivision of the trigeminal foramen into separate anterior and posterior openings for the maxillary (V2) and mandibular (V3) branches of the trigeminal nerve (CN V), respectively (Fig. 7A; Caldwell, 2019; Maisano and Rieppel, 2007). This lateral separation of the trigemino-facialis chamber (*sensu* Maisano and Rieppel, 2007; Rieppel, 1979) into separate exits is accomplished by the laterosphenoid, a broad ossification separating the smaller anterior V2 foramen from the larger posterior V3 foramen (Figs 6C, 7A). The anterior trigeminal foramen (V2) is completely surrounded by the prootic, with no contribution from the parietal to its anterior border (Figs 6A, 7A). A small foramen—likely transmitting the hyomandibular branch of the facial nerve (CN VII)—is present within the V3 trigeminal foramen (Rieppel, 1979), extending dorsomedially into the otic capsule from the internal dorsal surface of the V3 foramen (Fig. 7A).

Two smaller foramina are present ventral to the trigeminal openings (Figs 6A, 7A). The posteriormost of these smaller foramina is just dorsal to the posterior opening of the Vidian canal, connected to this latter opening by a recess along the ventral border of the prootic (Figs 6A,C, 7A). This foramen leads dorsally into the trigemino-facialis chamber and transmits the palatine branch of the facial nerve (Fig. 7A,C; Rieppel, 1979). Underwood and Kochva (1993) also note this foramen as transmitting the protractor pterygoidei and quadrati nerves. The final foramen on the lateral surface of the prootic is at the base of the laterosphenoid ossification (Figs 6A,C, 7A). This represents the laterosphenoid foramen (Fig. 7A), which transmits branches of the cid (constrictor internus dorsalis)-nerve to innervate the cid-musculature complex, including the levator pterygoidei nerve (Rieppel, 1979; Rieppel and Maisano, 2007; Underwood and

For Peer Review Only

Kochva, 1993). It is internally forked, leading anteroventrally to a small foramen located midway along the internal prootic-parabasisphenoid suture and leading posterodorsally into the trigemino-facialis chamber.

The trigemino-facialis chamber opens internally via a large foramen at the base of the medial surface of the prootic (Fig. 7B). Posterodorsally to this medial opening, two other foramina are present on the medial surface of the prootic (Fig. 7B). The larger and posteriormost of these is the foramen for the acoustic nerve (CN VIII) (Rieppel and Maisano, 2007), anterior to which lies a smaller foramen allowing passage of the facial nerve (CN VII) into the otic capsule (Fig. 7B).

The posterior surface of the prootic contains an elaborate cavity housing the anterior portions of the otic capsule and semicircular canals (horizontal and anterior), which lie posterodorsal to the trigemino-facialis chamber (Fig. 7D). The anterior part of the stapedial footplate rests within the lateral portion of this cavity, covering the fenestra ovalis (Fig. 7D; fenestra vestibuli *sensu* some authors, e.g., Maisano and Rieppel, 2007; Rieppel and Zaher, 2001). The fenestra ovalis itself is visible within the prootic as a slight dorsoventral constriction of the otic capsule in posterior view (Fig. 7D). The gap between the fenestra ovalis and stapedial footplate medially and the wall of the braincase laterally forms the juxtastapedial recess (Fig. 7D). Interestingly, whereas the prootic typically forms the anterior border of the circumstapedial opening in snakes bearing a ‘crista prootica’ (the anterior component of the crista circumfenestralis; CCF), in FMNH 62204 the prootic is excluded from this border by an anterior bony bridge of the otoccipital (Figs 6A,C, 7H,L); a ‘crista prootica’ as typically seen in the CCF of snakes is therefore absent.

For Peer Review Only

3.4.4. Supraoccipital

The supraoccipital is a median element composed of a flat roof with a complex descending process on each lateral margin (Fig. 7E–G). The dorsal surface of the supraoccipital bears a slight sagittal crest toward its anterior extent, with slight depressions on either side of the midline (Figs 1B, 7E). The aforementioned descending processes are ventrolaterally excavated so as to surround the dorsal portion of the otic capsules (Fig. 7G). Each descending process bears three foramina: one anterior and one posterior for the passage of the anterior and posterior semicircular canals, and one medially representing the endolymphatic foramen (Fig. 7G). The two semicircular canals meet at the common crus within the supraoccipital.

3.4.5. Otoccipital

The otoccipital results from a fusion of the opisthotic and exoccipital bones. Each otoccipital bears a posterior projection from its posteroventral corner which forms the lateral component of the occipital condyle (Figs 6A–C, 7H–I,K–L). On the external surface of the otoccipital, a groove separates the occipital condyle from the rest of the otoccipital (Fig. 7L), confluent with the groove externally surrounding the basioccipital portion of the occipital condyle (Fig. 6H).

The anterior surface of the otoccipital bears a deep cavity housing the posterior portions of the otic capsule and semicircular canals (horizontal and posterior) (Fig. 7I,J). In anterior view, the otic capsule is delimited laterally by the stapedial footplate, which sits in the fenestra ovalis surrounded laterally by the juxtastapedial recess (Fig. 7J).

The lateral surface of the otoccipital bears five openings visible in lateral view (Fig. 7H). The anteriormost of these is the circumstapedial opening (i.e., the lateral opening of the juxtastapedial recess) (Fig. 7H,L). The juxtastapedial recess is the gap between the stapedial

For Peer Review Only

footplate and the lateral wall of the braincase, surrounded by an elaboration of three crests—the cristae prootica, interfenestralis, and tuberalis—which form the crista circumfenestralis (CCF) (Palci and Caldwell, 2014). In its fully developed form (Type 4 *sensu* Palci and Caldwell, 2014), the CCF in turn obscures the stapedial footplate and lateral aperture of the recessus scalae tympani (LARST, also called the fenestra rotunda by some authors) in lateral view (Palci and Caldwell, 2014). In *Atractaspis irregularis*, the 'crista prootica' as traditionally conceived is absent; whereas the crista prootica typically forms the anterior border of the circumstapedial opening (Palci and Caldwell, 2014), in *A. irregularis* the otoccipital instead bears a bridge of bone delimiting this anterior border, thus contributing to the anterior enclosure of the juxtastapedial recess and excluding the prootic (Figs 6A,C, 7H,L). Within the juxtastapedial recess and obscured in lateral view, the LARST occurs just posteroventral to the fenestra ovalis and stapedial footplate. The crista interfenestralis separates the LARST from the fenestra ovalis, though is also hidden in lateral view. This is typical of the CCF in its most extreme form, i.e., Type 4 (Palci and Caldwell, 2014). The crista tuberalis is the final component of the CCF, separating the LARST anteriorly from the jugular foramen posteriorly (Fig. 7H,L). In *A. irregularis*, this crest forms the posterior rim of the juxtastapedial recess, surrounding the posterior portion of the stapedial footplate and partially hiding the jugular foramen in lateral view (Figs 6A,C, 7H,L).

The second opening on the lateral wall of the otoccipital is the jugular foramen, located just posterior to the crista tuberalis and internally subdivided into two smaller foramina (Fig. 7H,L). The glossopharyngeal (CN IX) and vagus (CN X) nerves presumably pass through this foramen (Rieppel, 1979; Rieppel and Zaher, 2001; Young, 1987).

For Peer Review Only

Three more foramina on the lateral surface of the otoccipital, posterior to the jugular foramen, represent exits for branches of the hypoglossal nerve (CN XII) (Fig. 7H).

The internal surface of the otoccipital bears a cluster of four large foramina close to the suture with the basioccipital (Fig. 7I). The foramen located most anterodorsally in the cluster corresponds to the medial counterpart of the jugular foramen (Fig. 7I). The foramen located near the anteroventral corner of the otoccipital represents the medial aperture of the recessus scalae tympani (Fig. 7I). The two foramina located posteroventral to the jugular foramen represent openings for branches of the hypoglossal nerve (Fig. 7I). A small foramen piercing the lateral border of the foramen magnum represents the posteriormost branch of the hypoglossal nerve (Fig. 7I).

3.4.6. Stapes

The stapes is a very thin element composed of the stapedial shaft attached to an expanded footplate (Fig. 7M–O). In *Atractaspis irregularis*, the stapedial footplate is anteriorly expanded so as to broadly underlie the prootic within the juxtastapedial recess. The stapedial shaft projects posterolaterally from midheight on the stapedial footplate through the circumstapedial opening of the juxtastapedial recess (Figs 6A,C, 7N). In FMNH 62204, the stapedial shaft is very short and does not extend external to the juxtastapedial recess (Figs 6A,C). This condition occurs among most of the *Atractaspis* individuals examined (*A. aterrima*; *A. bibronii*, *A. corpulenta* – MCZ R-4826, *A. dahomeyensis*; *A. irregularis irregularis*; *A. irregularis parkeri*; *A. microlepidota microlepidota*); however, in a specimen of *A. bibronii* (MCZ R-190390) and in one of *A. microlepidota* (FMNH 58397), the stapedial shaft extends toward the midpoint of the quadrate shaft (C.S. and A.P, pers. obs.). This reduction of the stapedial shaft in most specimens likely reflects the presence of intervening cartilage connecting the ossified stapes to the quadrate.

For Peer Review Only

Interestingly, in colubroids, the cartilaginous component of the quadrate-stapes articulation is typically limited to cartilaginous caps on the stapedial shaft and quadrate articulatory process (see Caldwell, 2019:fig. 3.15). The presence of an elongate stapedial shaft in specimens of *A. bibronii* and *A. microlepidota* is consistent with this colubroid condition. Although the stapedial shaft may be easily broken off in specimens from dry skeletal collections, the short shaft is certainly genuine in the micro-CT scanned specimens of *Atractaspis* examined (*A. aterrima*, *A. irregularis*, *A. microlepidota microlepidota*).

3.5. Suspensorium and Mandible

3.5.1. Supratemporal

The supratemporal is a thin, anteriorly downcurved element articulating medially with the prootic and otoccipital and laterally with the quadrate (Figs 8A, 9K–L). The supratemporal of *Atractaspis irregularis* is quite reduced compared to other derived alethinophidians, as it does not extend posteriorly beyond the occiput as in booids and some caenophidians (e.g., *Thamnophis radix* and *Homalopsis buccata*) and does not extend anteriorly onto the parietal as in other caenophidians (e.g., *Afronatrix anoscopus*, *Coluber constrictor*, *T. radix*), instead articulating only with the prootic and otoccipital (Fig. 1B). Reduction of the supratemporal occurs in several other fossorial snakes, with scolecophidians exemplifying the most extreme modification of the supratemporal to either a vestigial splint of bone (e.g., *Liotyphlops albirostris*, *Typhlophis squamosus*) or more commonly to being entirely absent (e.g., *Leptotyphlops dulcis*, *Typhlops jamaicensis*, *Anomalepis aspinosus*, *Anomalepis mexicanus*). The supratemporal is also absent in the genus *Uropeltis* (C.S., pers. obs.; Olori and Bell, 2012) and in

For Peer Review Only

Anomochilus leonardi (though is present in *A. weberi*) (C.S., pers. obs.; Rieppel and Maisano, 2007).

3.5.2. Quadrate

The quadrate in *Atractaspis irregularis* is a curved rod articulating dorsally with the supratemporal and ventrally with the compound bone (Fig. 8A). As is typical of caenophidians, the quadrate is angled distinctly posteroventrally, such that the quadrato-mandibular joint is well posterior to the occipital condyle (Fig. 1A–B, 8A). This elongate and posteriorly angled form of the quadrate is quite distinct compared to other fossorial snakes, in which the quadrate is either short and vertical (e.g., *Anilius scytale*, *Cylindrophis ruffus*, *Loxocemus bicolor*, *Xenopeltis unicolor*, *Casarea dussumieri*), short and vertical but displaced anteriorly with a large and posteriorly extending suprastapedial process (e.g., *Anomochilus leonardi*, *Uropeltis woodmasoni*, *U. melanogaster*), or elongate but angled anteriorly (as in scolecophidians, e.g., *Liotyphlops albirostris*, *Typhlophis squamosus*, *Typhlops jamaicensis*). The cephalic condyle is confluent with the quadrate shaft and tapers to a rounded anterodorsal terminus (Fig. 9A–B), whereas in other colubroids it is a distinctly expanded process (e.g., *Afronatrix anoscopus*, *Thamnophis radix*, *Coluber constrictor*, *Diadophis punctatus*, *Naja naja*). Ventrally, the mandibular condyle of the quadrate forms a saddle-shaped joint which articulates with the mandibular condyle of the compound bone (Figs 8A, 9A–B). The lateral surface of the quadrate is smooth (Fig. 9A), whereas the medial surface bears a slight overhanging crest delimiting the posterodorsal extent of its articulation with the supratemporal (Fig. 9B). A small articulatory process is present medially at about midheight for articulation with the stapes or its cartilaginous extension (Fig. 9B).

For Peer Review Only

3.5.3. Compound Bone

As is typical of snakes, the compound bone is a long, slightly bowed, edentulous rod that comprises the majority of the mandible (Figs 8, 9E–J). Posteriorly, the compound bone bears a saddle-shaped mandibular condyle that articulates with the mandibular condyle of the quadrate (Figs 8, 9E–F,I–J). A foramen for the chorda tympani nerve (CNVII) is present on the dorsomedial surface of the compound bone, just anterior to the articular joint with the quadrate (Fig. 9J). The retroarticular process is essentially absent, similar to the condition in other burrowing snakes such as *Cylindrophis ruffus*, *Anilius scytale*, and *Calabaria reinhardtii*, but in contrast to the pronounced retroarticular process typical of scolecophidians (e.g., *Liotyphlops albirostris*, *Typhlophis squamosus*, *Typhlops jamaicensis*). The mandibular or adductor fossa occurs about midway along the dorsal margin of the compound bone, leading anterolaterally into a foramen and anteriorly into the Meckelian canal (Fig. 9E,G–H,J). The Meckelian canal is completely surrounded by the compound bone posteriorly, whereas anteriorly it is delimited by the compound bone laterally and by the angular medially (Figs 8B, 9F,I). The compound bone tapers anteriorly to articulate with the deeply notched posterior terminus of the dentary (Figs 8, 9G,J).

3.5.4. Dentary

The dentary of *Atractaspis* is quite unique compared to other, non-fossorial colubroids. As is common in fossorial snakes (e.g., *Uropeltis melanogaster*, *U. woodmasoni*, *Typhlops jamaicensis*, *Leptotyphlops dulcis*, *Liotyphlops albirostris*; but not *Cylindrophis ruffus*, *Anilius scytale*, *Anomochilus leonardi*, or *Calabaria reinhardtii*), the mandible is underslung relative to the rest of the skull, causing the snout complex to project prominently anterior to the mandible (Figs 1A, 8A). The dentary is markedly slim and rod-like (Figs 8, 9C–D), similar to the

For Peer Review Only

compound bone and in contrast to the more robust mandible of other colubroids (C.S., pers. obs.; see also Palci et al., 2016; Racca et al., 2020; Scanferla, 2016; Strong et al., 2019). The dentition is also highly reduced, with the dentary of *Atractaspis* species typically bearing only two small teeth (Deufel and Cundall, 2003), with a maximum of four (Berkovitz and Shellis, 2017). The dentary is edentulous in the specimen of *A. irregularis* illustrated here, though this is likely the result of postmortem tooth loss as two tooth sockets are present. The dentary tapers anteriorly to a thin, medially curved apex (Fig. 9C–D). The posterior terminus of the dentary bears three prongs: two dorsally, which form a fork overlying the dorsal margin of the compound bone (Figs 8, 9C), and one ventrally, which articulates with the compound bone dorsolaterally and the splenial dorsomedially (Figs 8, 9D). The dentary completely encloses the Meckelian canal anteriorly, whereas posteriorly the splenial forms the medial wall of the Meckelian canal (Figs 8B, 9D). A mental foramen is not evident, representing a state unique to *Atractaspis* relative to all other snakes except some scolecophidians (anomalepidids and some typhlopids; Caldwell, 2019).

3.5.5. Angular

The angular is a roughly triangular bone overlying the Meckelian canal on the medial surface of the compound bone (Fig. 8B). The angular is smooth medially (Fig. 9N) but grooved laterally in order to accommodate the Meckelian canal (Fig. 9M). The angular is pierced midway along its length by the posterior mylohyoid foramen (Fig. 9M–N). Along its dorsal margin, the angular bears a broad emargination such that the Meckelian canal is slightly exposed at this position along the compound bone (Figs 8B, 9M–N). The angular tapers posteriorly to a thin apex (Fig. 9M–N). Anteriorly, the dorsal margin of the angular extends further than the ventral

For Peer Review Only

margin, corresponding to and articulating with the posteroventral tapering of the posterior terminus of the splenial (Fig. 8B).

3.5.6. Splenial

The splenial is a thin, triangular bone that overlies the Meckelian canal along the dentary and anteriormost extent of the compound bone (Fig. 8B). Its medial surface is smooth (Fig. 9P), whereas its lateral surface bears a V-shaped groove—beginning near the midpoint of the splenial and continuing posteriorly onto the lateral surface of the angular—that surrounds the medial surface of the Meckelian canal (Fig. 9O). The anterior mylohyoid foramen creates an oblong opening leading into the Meckelian canal near the posterior terminus of the splenial (Figs 8B, 9O–P). The splenial tapers anteriorly to articulate with a medial groove on the dentary, whereas posteriorly it articulates with the angular, tapering such that its ventral margin extends farther posteriorly than its dorsal margin (Figs 8B, 9O–P).

4. Discussion

4.1. Adaptations for Fossoriality

The overall morphology of the skull of *Atractaspis irregularis* is markedly different from that of other colubroids. This unique structure is due in part to heterochrony (see §4.2 and §4.3), but is also due largely to several adaptations for fossoriality. Principal among these are reduction of the orbits (§3.2.1), modification of the jaws (§3.3 and §3.5), and increased integration of the snout complex (§3.1).

The mandible is underslung relative to the rest of the skull, a condition that occurs in many other fossorial snakes (Figs 1A, 8A; §3.5.4). This reduction aids in limiting resistance and

For Peer Review Only

preventing the jaws from being forced open while burrowing or moving in constricted areas (Wake, 1993). This reduction of the mandible likely also explains the absence of the mental foramen, as similar absence in scolecophidians has been linked to decreased importance of the labial glands (Caldwell, 2019).

The maxilla is also unique in its anatomy and biomechanics of fang rotation. Although the maxilla and dentition are superficially similar to the condition in viperids (e.g., *Bothrops asper*, *Agkistrodon contortrix*), key differences such as the structure of the maxilla-prefrontal articulation strongly suggest these similarities to be convergent (Kochva, 1987). In the aforementioned viperids, the articulating surfaces of these elements are smooth, with several ligaments and muscles for control and stabilization of the maxilla (Kochva, 1987). In contrast, the anterodorsal surface of the maxilla of *Atractaspis irregularis* is complexly integrated with the prefrontal (Figs 1, 4, 5). This difference in morphology implies a difference in function; rather than relying on ligamentous stabilization of the maxilla as in viperids, the complex ball-and-socket-like articulation of the maxilla-prefrontal in *Atractaspis* provides structural support and limits rotation of the maxilla and fangs to a ventrolateral-dorsomedial axis (Deufel and Cundall, 2003; Kochva, 1987; see the former for a detailed examination of functional morphology and feeding mechanisms in *Atractaspis*). Ultimately, rather than the jaws fully opening and the fang swinging ventrally, *Atractaspis* is characterized by a unique 'side-stabbing' movement in which the fang protrudes ventrolaterally from the side of the closed mouth (Deufel and Cundall, 2003; Kochva, 1987; Underwood and Kochva, 1993). This phenomenon is facilitated by the underslung or countersunk mandible and is used to envenomate prey via posteroventral movement of the head (Deufel and Cundall, 2003; Kochva, 1987; Underwood and Kochva, 1993), which aids prey envenomation in restricted spaces such as burrows (Deufel and Cundall,

For Peer Review Only

2003; Shine et al., 2006). Alongside the reduction of the mandible, this modification to the palatomaxillary arch demonstrates the role of fossoriality in driving adaptations involving complex morphofunctional systems such as macrostomy.

Another important adaptation for fossoriality involves the naso-frontal joint. In *Atractaspis irregularis*, this joint involves the tightly integrated snout complex—composed of the nasals, premaxilla, septomaxillae, and vomers—itself in extensive articulation with the medial frontal flanges (i.e., the fused medial frontal pillars and subolfactory processes of the frontal) (Figs 1, 2, 3G). This contact contrasts typical, non-fossorial macrostomatans as described by Rieppel (2007), in which the nasal contacts either the medial frontal pillars or the frontal subolfactory processes but not both. In particular, in typical colubroids the nasals tend to contact the frontals ventrally at the subolfactory processes, with the septomaxillae forming the main connection between the snout complex and frontals; in some cases the nasals are completely excluded from contact with the frontals, and the connection between the latter and the snout complex occurs exclusively via the septomaxilla (Rieppel, 2007).

The naso-frontal configuration in *Atractaspis* exemplifies the 'central rod design' of the naso-frontal joint in fossorial snakes, in which forces associated with burrowing are transmitted from the snout to the frontals via the articulation of the premaxilla, nasals, and medial frontal flanges (Fig. 10A; Cundall and Rossman, 1993; Rieppel, 2007). As initially described by Cundall and Rossman (1993), this 'central rod design' is one of two main configurations associated with transmission of force from the snout complex in burrowing snakes. The other configuration—termed the 'outer shell design'—involves the transmission of force along the outer margins of the skull, via extensive contact along the dorsal and lateral margins of the premaxilla, nasals, prefrontals, and frontals (Fig. 10E; Cundall and Rossman, 1993; Rieppel et

For Peer Review Only

al., 2009). Although these configurations were originally described as characterizing uropeltines and scolecophidians, respectively (Cundall and Rossman, 1993), the 'central rod design' has since been expanded to encompass all burrowing alethinophidians based on its reliance on the medial frontal pillars, which are absent in scolecophidians (Rieppel, 2007; Rieppel et al., 2009; Rieppel and Maisano, 2007).

Rieppel and Maisano (2007) used this absence of the medial frontal pillars as evidence refuting scolecophidians as 'regressed macrostomatans'. Coined by Rieppel (2012), this hypothesis of 'regressed macrostomy' places scolecophidians as nested within the Alethinophidia, having secondarily lost the anatomical requirements for macrostomy (Caldwell, 2019; Harrington and Reeder, 2017; Kley, 2006), in contrast to their traditional placement as a plesiomorphic group diverging basally among extant snakes (e.g., Bellairs and Underwood, 1951; List, 1966; Miralles et al., 2018; Rieppel, 1988, 2012; Walls, 1942). This 'regressive' evolution is typically attributed to paedomorphosis (Caldwell, 2019; Kley, 2006), a developmental phenomenon in which embryonic or juvenile morphologies of an ancestral taxon are retained in the adult morphology of a descendant taxon (Hanken and Wake, 1993; McNamara, 1986). Arguing against this hypothesis, Rieppel and Maisano (2007) concluded that paedomorphic modification of a macrostomatan skull could result in a skull similar to that of *Anomochilus* for example, in which the medial frontal pillars are still essential to the naso-frontal joint (Fig. 10C), but could not reasonably result in a scolecophidian skull, in which the medial frontal pillars are absent and force is transmitted entirely along the outer margins of the snout elements and frontal (Fig. 10D,E). However, this conclusion warrants re-examination, especially in light of *Atractaspis* and the closely related taxon *Aparallactus* (see below).

For Peer Review Only

Essentially, the concept that the 'central rod' and 'outer shell' designs are fundamentally incompatible does not recognize the numerous examples of gradation between these morphologies in various taxa (Fig. 10). For example, *Anomochilus*—used by Rieppel and Maisano (2007) as an exemplar of the 'central rod design'—in fact incorporates elements of both naso-frontal morphologies (Fig. 10C). As recognized by Cundall and Rossman (1993) in their initial description of these designs, the medial frontal pillars are present in *Anomochilus* to transmit force via the medial nasal flanges, but the dorsal laminae of the nasals are also expanded and articulate with the prefrontals to transmit force dorsally and laterally to the frontals (Fig. 10C; see also Cundall and Rossman, 1993:fig. 25C).

Furthermore, Rieppel et al. (2009) describe the scolecophidians *Liotyphlops* and *Leptotyphlops* as incorporating features of a 'central rod design'. In *Liotyphlops*, this partial 'central rod design' consists of a contact between the nasal and the frontal not only dorsally (as in typhlopids) but also ventrally, below the olfactory tracts. In *Leptotyphlops*, it is the expanded posterior processes of the septomaxillae that abut ventrally against the subolfactory processes of the frontals (Fig. 10D), a contact described by Rieppel (2007) as generally typical of colubroids. Rieppel et al. (2009) further describe the mixture of 'outer shell' and 'central rod' components in *Leptotyphlops* as a potentially plesiomorphic condition for scolecophidians, with typhlopids subsequently specializing into the idealized 'outer shell design' (Fig. 10E) and anomalepidids (e.g., *Liotyphlops*) developing a unique version of a 'central rod design'.

Finally—and perhaps most relevant here given its frequent recovery as a close relative of *Atractaspis* (Gauthier et al., 2012; Portillo et al., 2018; Portillo et al., 2019; Underwood and Kochva, 1993; Vidal et al., 2008; Zaher et al., 2009)—*Aparallactus* has been noted as exhibiting a more 'outer shell'-like than 'central rod'-like morphology (Rieppel, 2007). For example, the

For Peer Review Only

medial frontal pillars are quite narrow anteroposteriorly, more closely approaching the condition in *Anomochilus* than in *Atractaspis* (C.S., pers. obs., *Anomochilus leonardi*, *Aparallactus modestus*, *Aparallactus guentheri*, *Aparallactus werneri*, *Atractaspis irregularis, Atractaspis microlepidota*). The nasals are also broader than in *Atractaspis* or *Uropeltis* and articulate laterally with the prefrontals, unlike in *Atractaspis* (Fig. 10B).

From these observations and discussions of the naso-frontal joint and its evolutionary implications, it is clear that the 'outer shell' and 'central rod' designs are not fundamentally incompatible. Rather, there is extensive gradation between these morphologies, with certain scolecophidians (e.g., *Leptotyphlops* and *Liotyphlops*) exhibiting 'central rod'-like morphologies and certain alethinophidians (e.g., *Anomochilus* and *Aparallactus*) exhibiting 'outer shell'-like morphologies (Fig. 10).

To co-opt the transformational scenario of Rieppel et al. (2009)—in which *Leptotyphlops* is hypothesized as ancestral to the typhlopid and anomalepidid conditions—the aforementioned taxa (i.e. *Atractaspis*, *Anomochilus*, and *Aparallactus*) provide insight into earlier stages of this proposed evolutionary scenario. Altogether, these taxa illustrate a possible transition from a typical alethinophidian 'central rod design' (as in *Atractaspis*; Fig. 10A), to a scolecophidian-like alethinophidian condition (as in *Aparallactus* or *Anomochilus*; Fig. 10B,C), to an alethinophidian-like scolecophidian condition (as in *Leptotyphlops*; Fig. 10D), and finally to a typical scolecophidian 'outer shell design' (as in typhlopids; Fig. 10E). Note that this is not a proposal of explicit ancestor-descendant relationships among these taxa, but rather a discussion of how these broader morphotypes grade into one another and therefore represent a morphological spectrum between two endpoint morphologies, i.e., the 'outer shell' and 'central rod' designs.

For Peer Review Only

As presented by Rieppel and Maisano (2007), a major obstacle precluding an alethinophidian origin of scolecophidians is the absence of the medial frontal pillars in scolecophidians. This absence has been hypothesized as primitive in scolecophidians based on similar absence in non-ophidian squamates and *Dinilysia* (Rieppel, 1978). However, this putative fundamental difference becomes much less restrictive in light of the extensively paedomorphic and autapomorphic condition of the scolecophidian skull in general. That is, given the high degree of paedomorphosis suggested in the scolecophidian skull (see §4.2 and §4.3), combined with the functional constraints and pressures associated with fossoriality (Maddin et al., 2011; Wake, 1986), the potential loss of the medial frontal pillars is in fact a relatively minor evolutionary transformation. Scolecophidians have lost entire bones relative to other squamates, such as the supratemporal (see §3.5.1), yet this does not preclude their derivation from a supratemporal-bearing squamate ancestor; similarly, the absence of the medial frontal pillars should not automatically preclude derivation from a pillar-bearing (i.e., alethinophidian) ancestor.

In fact, Rieppel and Maisano (2007) were the first to notice that the lack of medial frontal pillars and a laterosphenoid in scolecophidians could easily reflect paedomorphosis. Developmental studies have shown that the frontals of snakes start developing as paired ossifications on the sides of the skull that only later in development merge along the midline (e.g., Boughner et al., 2007; Polachowski and Werneburg, 2013); this implies that the medial flanges are the last feature to ossify and could easily fail to form due to truncations in development (i.e., paedomorphosis). The lack of a laterosphenoid may similarly result from a delay in skull ossification, as the subdivision of the trigeminal foramen into anterior and

For Peer Review Only

posterior compartments occurs very late in development (Khannoon and Evans, 2015; Khannoon et al., 2020).

Despite their initial argument about paedomorphosis, though, Rieppel and Maisano (2007) further discuss the highly modified and expanded snout complex of scolecophidians as refuting the idea of this group being derived from an alethinophidian ancestor. However, this autapomorphic condition represents a morphological novelty that, following the 'null hypothesis' of miniaturization presented by Hanken (1984), clearly relates to the specialized miniaturized and fossorial nature of this group (Hanken, 1984; Hanken and Wake, 1993; Wake, 1986). This is especially true in light of the morphological gradation of the naso-frontal joint in fossorial snakes as presented above (Fig. 10). As Hanken and Wake (1993) and Rieppel (1996) discuss, this novelty is often superimposed overtop paedomorphic features in miniaturized taxa, resulting in a complex mixture of autapomorphies related to heterochrony, miniaturization, and fossoriality in these organisms. This certainly seems to be the case in *Anomochilus* and *Aparallactus*, both burrowing and miniaturized, and both showing an expanded snout complex similar to that of scolecophidians, with extensive contact between broadened nasals and prefrontals (Fig. 10).

Certain autapomorphic features of the scolecophidian snout—including the absence of the medial frontal pillars—are further consistent with the loss of the prokinetic joint in these snakes. Modification of the prokinetic joint has similarly been noted as an adaptation for greater structural integrity in the skull of other burrowing snakes, such as uropeltids and *Eryx* (Rieppel, 1978). Altogether, these observations indicate that an 'outer shell design' of the naso-frontal joint as is characteristic of scolecophidians can reasonably be derived from an alethinophidian ancestor, contrary to previous arguments.

For Peer Review Only

4.2. Heterochronic Modification of the Jaws, Palate, Suspensorium, and Braincase

The jaws and palate of *Atractaspis* are distinctly reduced compared to non-fossorial colubroids (Fig. 11A). The pterygoid in particular has an elongate, rod-like shape which also occurs in many other fossorial taxa, especially scolecophidians (Figs 5A–D, 11; §3.3.1); however, unlike scolecophidians, the pterygoid of *A. irregularis* projects well posterior to the occiput (Figs 1, 11A), as is typical of 'macrostomatan' (i.e., large-gaped) snakes (C.S., pers. obs.; see also Palci et al., 2016; Scanferla, 2016; Strong et al., 2019). The number of teeth on all typical tooth-bearing elements is highly reduced, so as to be completely absent on the pterygoid and with only a few teeth on the palatine, dentary, and maxilla (Figs 1, 11). The compound bone also exhibits a simple, rod-like form, lacking features such as a surangular crest or well-developed retroarticular process (Figs 1, 8, 9E–J, 11).

This widespread reduction is consistent with paedomorphosis. In other words, the reduced forms of the mandibular and palatal elements in *Atractaspis irregularis* adults reflect retention of the simple, poorly-developed conditions of these elements in earlier ontogenetic stages in related taxa. In this case, we can infer the plesiomorphic developmental pathways of these elements using the ontogenetic trajectories of closely related species. In embryos of the viperid *Bothropoides jararaca*, the pterygoid maintains a simple, rod-like form until SES stage 4 (i.e., mid-stage embryonic development), at which point it elaborates in form before teeth begin developing from SES stages 6 to 7 (i.e., late-stage embryonic development) (Polachowski and Werneburg, 2013). Similar developmental timing characterizes the dentary and palatine in this species (Polachowski and Werneburg, 2013). Khannoon and Evans (2015) describe similar timing for these elements in the elapid *Naja haje haje*. Finally, in late-stage embryos of the colubrid *Thamnophis radix*, the mandibular and palatal elements already bear teeth and are much

For Peer Review Only

more elaborate in form than in adults of *A. irregularis* (Strong et al., 2019). *A. irregularis* is therefore clearly paedomorphic relative to other colubroids regarding the morphology of the mandible and palate, as adults of this species exhibit the conditions present in mid-stage and earlier embryos of surrounding colubroid taxa. This paedomorphosis heavily contributes to the specialized morphology of *Atractaspis* within this larger clade.

This mechanism of heterochrony has been proposed for comparable adaptations in other snakes. These include reduction of the palatal bones and dentition in *Anomochilus* and uropeltine snakes, and reduction of the retroarticular process of the compound bone in *Anomochilus* (Rieppel and Maisano, 2007). Most prominently, scolecophidians—blind, miniaturized, fossorial snakes—have been noted as paedomorphic with respect to the mandible, palatomaxillary complex, and suspensorium (Caldwell, 2019; Kley, 2006).

In fact, the paedomorphosis exhibited by scolecophidians is in many ways comparable to that of *Atractaspis*—e.g., the reduced mandible and highly reduced and often absent dentition (Caldwell, 2019; Kley, 2006)—though in other aspects it is far more extensive than that noted herein for *Atractaspis* (Fig. 11). For example, the proximal epiphysis of the quadrate remains unfused (Kley, 2006), the ectopterygoid and supratemporal are typically completely absent or at least extremely reduced (Caldwell, 2019; Chretien et al., 2019; Rieppel et al., 2009), and the quadrate is oriented anteriorly, representing an extreme retention of the embryonic squamate condition (Caldwell, 2019; Hernández-Jaimes et al., 2012; Kamal, 1966; Kley, 2006; Rieppel and Zaher, 2000; Scanferla, 2016). Similar reduction and anterior displacement of the suspensorium occurs in other miniaturized snakes, such as *Anomochilus* and *Uropeltis* (§3.5.1 and §3.5.2; see also Olori and Bell, 2012). These taxa altogether reflect a trend toward extensive

For Peer Review Only

paedomorphic modification of the suspensorium and jaws in miniaturized vertebrates (Hanken and Wake, 1993; Olori and Bell, 2012).

Evidence of paedomorphosis can also be found in the overall shape of the braincase of snakes such as *Atractaspis*, *Anomochilus*, and scolecophidians, in which the external surface of the braincase appears smooth and rounded, devoid of any sharp crests or ridges, a condition resembling that of neonate or juvenile snakes (Palci et al., 2016; Strong et al., 2019). The braincase is also relatively large in *Atractaspis* compared to adults of other colubroids (e.g., *Thamnophis*), a feature again resembling the condition among juvenile snakes (Palci et al., 2016; Strong et al., 2019). The lack of a well-developed dorsum sellae overhanging the sella turcica in *Atractaspis*, *Anomochilus*, and scolecophidians may represent another paedomorphic feature, related to the lack of crests and ridges on the external surface of the braincase.

However, not all heterochronic changes to the skull of *Atractaspis* involve paedomorphosis. Certain features—such as the quadrate, the snout complex, and the parasphenoid rostrum of the parabasisphenoid—in fact exhibit peramorphosis (i.e., extended development; McNamara, 1986) relative to other colubroids such as *Thamnophis radix* (Fig. 11A). In the case of the parasphenoid rostrum (Figs 6A–F, 11A) and the snout (Figs 2, 11A), this peramorphosis contributes to fossoriality, as these components are expanded and tightly integrated with surrounding elements, thus strengthening the skull (see also §4.1). The peramorphic extension of the quadrate in *Atractaspis* relative to other colubroids is likely related to reduction of the supratemporal: because the supratemporal of *Atractaspis* is much smaller and terminates farther anteriorly than in typical colubroids (Figs 1B, 8A, 9K–L, 11A; §3.5.1), the quadrate must therefore extend anteriorly in order to maintain a functional articulation with this element. For all of these skull components, peramorphosis essentially addresses functional

For Peer Review Only

constraints to the skull, related either to burrowing (as for the parasphenoid rostrum and snout complex) or to maintaining functionality of the suspensorium (as for the quadrate). A similar combination of paedomorphosis and peramorphosis, with this latter phenomenon compensating for functional requirements, has been noted throughout paedomorphic tetrapods (Rieppel, 1996; Wake, 1986).

Finally, the supratemporal of *Atractaspis irregularis* also provides insight into heterochrony in other colubroids. The supratemporal of *A. irregularis* does not extend anteriorly beyond the prootic or posteriorly beyond the occiput (Figs 1B, 11A), thus reflecting reduction and developmental truncation of this element relative to typical caenophidians and booids, respectively (Palci et al., 2016; Strong et al., 2019). Interestingly, this configuration of the supratemporal in *Atractaspis irregularis* matches that in embryos of the caenophidian *Thamnophis radix* (Strong et al., 2019). In contrast, the supratemporal in *T. radix* adults extends both anteriorly onto the parietal and posteriorly well beyond the occiput (Fig. 11A; Strong et al., 2019). This posterior projection is typically restricted to booids among 'macrostomatan' snakes, thus contrasting the typical condition proposed for caenophidians, in which the supratemporal does not extend significantly posterior to the occiput (Palci et al., 2016; Strong et al., 2019). In other words, the posterior elongation of this element throughout ontogeny in *T. radix* surpasses the condition typically present in adult caenophidians. Therefore, whereas *A. irregularis* exhibits paedomorphic modification of the supratemporal relative to other caenophidians, the supratemporal of *T. radix* exhibits peramorphosis relative to this clade.

Heterochrony therefore plays a major role in the evolution and development of the jaws, suspensorium, and overall skull shape in snakes.

For Peer Review Only

4.3. The Role of Heterochrony in the Evolution of Fossorial Snakes

Heterochrony has been proposed as one of the major forces driving the evolution of the ophidian skull from that of non-ophidian lizards (Da Silva et al., 2018; Hanken and Wake, 1993; Irish, 1989; Werneburg and Sánchez-Villagra, 2015). Studies of snake skull ontogeny are still relatively rare, tending to focus on embryonic development (e.g., Al-Mohammadi et al., 2020; Boback et al., 2012; Boughner et al., 2007; Jackson, 2002; Khannoon and Evans, 2015; Khannoon et al., 2020; Khannoon and Zahradnicek, 2017; Polachowski and Werneburg, 2013; Pringle, 1954; Sheverdyukova, 2017, 2019; Zehr, 1962), with only a few studies examining postnatal development (Palci et al., 2016; Scanferla, 2016; Scanferla and Bhullar, 2014; Sherratt et al., 2019; Strong et al., 2019; Young, 1989). However, our growing understanding of snake evolutionary development suggests that heterochrony is an important driver of the evolution not only of snakes relative to other squamates, but of snakes relative to each other (see also Da Silva et al., 2018). This importance is clearly supported by the extensive, heterochronic patterns of skull paedomorphosis and peramorphosis in several snake species, as discussed above.

Understanding the role of heterochronic processes in snake skull evolution is in turn essential for understanding snake phylogeny. Although scolecophidians are traditionally considered the most basal group of extant snakes, retaining many plesiomorphic non-ophidian squamate features (e.g., Bellairs and Underwood, 1951; List, 1966; Miralles et al., 2018; Rieppel, 2012; Walls, 1942), recent phylogenies have recovered scolecophidians as nested within the Alethinophidia (Fig. 12; Garberoglio et al., 2019; Palci and Caldwell, 2010). This placement of scolecophidians as highly modified alethinophidians is reminiscent of the aforementioned hypothesis of scolecophidians as ‘regressed macrostomatans’ (Caldwell, 2019; Harrington and Reeder, 2017; Kley, 2006). Because this latter perspective proposes heterochrony as a cause of

For Peer Review Only

this 'regressive' evolution (Caldwell, 2019; Kley, 2006), our observations of paedomorphosis in the jaws and suspensorium thus provide novel insight into this hypothesis of 'regressed macrostomy'.

As discussed above, *Atractaspis* and scolecophidians both exhibit paedomorphosis of various cranial elements, with this heterochrony being more extensive in the miniaturized scolecophidians than the fossorial but non-miniaturized *Atractaspis* (Fig. 11). For example, certain paedomorphic features (e.g., reduction of the mandible and dentition) occur in both groups, whereas other features (e.g., anterior orientation of the quadrate and marked reduction or loss of the supratemporal and ectopterygoid) occur only in scolecophidians (Fig. 11). These observations are consistent with the hypothesis that paedomorphosis causes—or at least strongly correlates with—miniaturization (Fröbisch and Schoch, 2009; Hanken, 1984; Sherratt et al., 2019; Wake, 1986). When considered in the context of these developmental phenomena, the morphologies of these fossorial taxa essentially fall along a continuum, with more 'extreme' paedomorphosis resulting in more 'extreme' anatomies.

This morphological and developmental gradation refutes the traditional concept of scolecophidians as fundamentally different from alethinophidians (Fig. 12A). Instead, miniaturization and paedomorphosis together represent a possible mechanism by which a scolecophidian-like morphology may be derived from a fossorially-adapted alethinophidian morphology, such as that of *Atractaspis* (Fig. 11A) or *Anomochilus* (Fig. 11B). Under this hypothesis, miniaturization and associated extensive paedomorphosis have superimposed many unique scolecophidian morphologies overtop the paedomorphic features already present in an ancestral fossorial alethinophidian morphotype (Fig. 11). Altogether, this morphological

For Peer Review Only

continuum therefore supports the recent hypothesis of an alethinophidian ancestry of scolecophidians (Fig. 12B; Caldwell, 2019; Garberoglio et al., 2019; Palci and Caldwell, 2010).

Of course, as is typical of miniaturized tetrapods, paedomorphosis alone does not account for all of the unique features of scolecophidians (Hanken and Wake, 1993; Rieppel, 1996). As noted above, other scolecophidian autapomorphies such as the greatly expanded snout instead represent adaptations related to fossoriality (List, 1966; Rieppel, 1996; Rieppel et al., 2009), exemplifying how ecological constraints can combine with miniaturization and paedomorphosis to create strikingly unique skull morphologies (Hanken and Wake, 1993; Rieppel, 1996). A similar combination of highly paedomorphic and highly autapomorphic features has been noted in other miniaturized, fossorial taxa, such as the caecilian *Idiocranium russeli* (Wake, 1986). As discussed for the naso-frontal joint (§4.1), Hanken's (1984) 'null hypothesis' of miniaturization establishes such occurrences of morphological novelty as being consistent with a hypothesis of paedomorphosis-driven miniaturization. We therefore propose that this combination of paedomorphic miniaturization and adaptational autapomorphy may underlie the evolution of the scolecophidian skull from an alethinophidian ancestor (Figs 11, 12).

As above (§4.1), it is important to emphasize that this is not an argument that scolecophidians are derived specifically from *Atractaspis*, nor that any of the anatomical similarities noted herein are synapomorphic. Indeed, given the well-documented homoplasy involved in adaptations related to fossoriality (Maddin et al., 2011; Savitzky, 1983) and paedomorphosis (Fröbisch and Schoch, 2009; Wiens et al., 2005), any similarity in the morphology of these taxa is quite conceivably convergent. Rather than a hypothesis of synapomorphy or of explicit phylogenetic relationships, this is instead a discussion and comparison of broad morphotypes, as exemplified by *Atractaspis* and scolecophidians. Thus, the

For Peer Review Only

core question presented herein is: if an *Atractaspis*-like morphotype can be derived from an alethinophidian ancestor, is it possible for a scolecophidian-like morphotype to also be derived from this lineage? In our view, burrowing adaptations in combination with heterochrony—specifically paedomorphosis, and in this case specifically related to the mandible and suspensorium—can reasonably be hypothesized as enabling derivation of the miniaturized and highly modified scolecophidian skull from an ancestral alethinophidian morphotype (Fig. 11).

For example, aside from *Atractaspis*, numerous similarities also exist between scolecophidians and the basal alethinophidian *Anomochilus*, such as the short, rod-like and toothless pterygoids, the laterally expanded nasals in contact with the prefrontals, a lateral contact between the nasal flanges and septomaxillae, the absence of a well-developed dorsum sellae overhanging the sella turcica, a rounded braincase, and an anteroventral tilt of the main axis of the quadrate (Figs 10, 11B). Unlike more derived alethinophidians, *Anomochilus* also shares with scolecophidians a reduced ectopterygoid (strongly reduced in Anomalepididae, absent in Leptotyphlopidae and Typhlopoidea; List, 1966; Rieppel et al., 2009) and the retention of the coronoid bone and vestigial pelvic girdle (Palci et al., 2020; Rieppel and Maisano, 2007).

Of course, this hypothesis of scolecophidians as ‘regressed alethinophidians’ requires rigorous testing. Primarily, any hypothesis of heterochrony requires a robust phylogenetic framework (Fröbisch and Schoch, 2009; Rieppel and Maisano, 2007; Wiens et al., 2005). However, the phylogeny of scolecophidians is uncertain, due in large part to disagreement between morphological and molecular data. Based on morphological evidence alone, scolecophidians would represent a monophyletic assemblage (Garberoglio et al., 2019; Gauthier et al., 2012; Hsiang et al., 2015). Molecular data, on the other hand, unequivocally support a paraphyletic “Scolecophidia”, with Leptotyphlopidae and Typhlopoidea as sister taxa and

For Peer Review Only

Anomalepididae in either a more basal or more derived position (e.g., Figueroa et al., 2016; Miralles et al., 2018; Zheng and Wiens, 2016). The conflicting placement of Anomalepididae relative to the other two scolecophidian lineages in molecular phylogenetic analyses is possibly affected by the early divergence of the group. The limitations of molecular phylogenetics in resolving the placement of early-diverging lineages (deep branches) have been highlighted in a recent study by Mongiardino Koch and Gauthier (2018).

The recovery of a robust scolecophidian phylogeny is also complicated by the fact that paedomorphosis itself may act as a confounding factor in phylogenetic analyses, both morphological and molecular (Hanken and Wake, 1993; Struck, 2007; Wiens et al., 2005). From a molecular perspective, paedomorphosis has been linked to extensive gene loss, as reported in a recent study on fish (Malmstrøm et al., 2018). This implies that the molecular signal from scolecophidian genomes may be significantly altered, and the absence of some putative alethinophidian autapomorphies (e.g., the duplicate control region in the mitochondrial genome; Dong and Kumazawa, 2005; Yan et al., 2008) could simply represent secondary losses rather than plesiomorphic conditions. It is also entirely possible that scolecophidian synapomorphies linking typhlopoids, leptotyphlopids, and anomalepidids have been lost for the same reason, a potential loss of phylogenetic signal that may contribute to the ambiguous placement of anomalepidids (e.g., Figueroa et al., 2016 vs Zheng and Wiens, 2016). If the scolecophidian genome is the result of simplification via gene loss, then this would have a profound effect on our ability to resolve their phylogenetic relationships based on molecular data alone.

In light of the potential importance of paedomorphosis, an examination of scolecophidian skeletal ontogeny is essential. The most accurate method of identifying paedomorphosis in scolecophidians would be via a comparative ontogenetic analysis incorporating scolecophidians,

For Peer Review Only

alethinophidians, and non-ophidian lizards. To our knowledge, only two such studies (Da Silva et al., 2018; Palci et al., 2016), both based in geometric morphometrics, have been conducted; in both cases, the results suggested scolecophidians as paedomorphic relative to other squamates. These studies indicate that this largely unexplored evolutionary scenario warrants further analysis, with large-scale sampling—both of taxa and of ontogenetic stages—key to robustly investigating this hypothesis.

Although a robust phylogenetic context is still lacking for snakes (Chretien et al., 2019), recently revised and large-scale datasets such as that of Simões et al. (2018) and Garberoglio et al. (2019) provide a sound basis for future large-scale studies of snake evolution. Interestingly, a recent morphological phylogeny (Garberoglio et al., 2019) focussing on extinct snakes recovered scolecophidians as nested within Alethinophidia (Fig. 12B), in stark contrast to the more orthodox placement of this group as basally divergent among Serpentes (Fig. 12A). These results strongly highlight the importance of continued morphological and phylogenetic analyses of this group, including a renewed examination of potential alethinophidian affinities of scolecophidians.

5. Conclusions

We herein present the first thorough description of the cranial osteology of *Atractaspis*, using fully segmented micro-CT scans of *A. irregularis* (Figs 1–9). This analysis reveals the jaws and suspensorium of *Atractaspis* to be paedomorphic relative to other colubroids. This observation in turn provides insight into the evolution of scolecophidian snakes, given the even more pronounced paedomorphosis hypothesized for this latter group (Fig. 11; Caldwell, 2019; Da Silva et al., 2018; Kley, 2006; Palci et al., 2016). Combined with our discussion of the naso-

For Peer Review Only

frontal joint in *Atractaspis* and other fossorial snakes (Fig. 10), our results contest the traditional view of scolecophidians as representing a primitive or ancestral morphology among snakes, instead lending support to the hypothesis of scolecophidians as 'regressed macrostomatans' (see Rieppel, 2012), or perhaps more precisely put, 'regressed alethinophidians' (Figs 11, 12). We propose that this 'regression' is the result of: paedomorphosis, to an extent beyond that present in *Atractaspis* (Fig. 11); miniaturization, which is tied to paedomorphosis and typically correlated with morphological novelty (Fig. 11; Hanken, 1984; Hanken and Wake, 1993); and adaptations for fossoriality, such as the structure of the naso-frontal joint, which combine with miniaturization to produce a highly autapomorphic skull morphology (Figs 10, 11; Hanken and Wake, 1993; Rieppel, 1996). Altogether, we hypothesize that these factors have driven the derivation of the scolecophidian skull from an alethinophidian ancestor.

Ultimately, this kind of transformational hypothesis is just that: a hypothesis, requiring robust evidence in order to be supported or refuted, and ultimately refined. This evidence can come in the form of anatomical observations and interpretations such as those we have presented in this study. A key line of evidence also lies in the phylogenetic analysis of the taxa in question. Such an undertaking warrants a treatment of its own and as such is outside the scope of this study; however, our descriptions, comparisons, micro-CT reconstructions, and preliminary examination of evolutionary scenarios provide an essential basis for future phylogenetic analyses. This is not a circular research program, but rather reflects the nature of scientific inquiry where each new answer generates numerous new questions further probing method, data, hypotheses, and theory. In particular, our observations and interpretations of the jaw, suspensorium, and naso-frontal joint in fossorial snakes raise intriguing possibilities regarding the phylogenetic placement of scolecophidians, thus contributing to recent discussions on the

For Peer Review Only

evolution of this group (e.g., Caldwell, 2019; Chretien et al., 2019; Miralles et al., 2018). These interpretations are especially relevant in light of recent phylogenies recovering scolecophidians as nested among alethinophidians (Garberoglio et al., 2019; Palci and Caldwell, 2010), in contrast to their traditional placement as the most basal living snakes (e.g., Hsiang et al., 2015; Longrich et al., 2012; Reeder et al., 2015).

Acknowledgements

We thank Luca Racca and another, anonymous reviewer for their comments regarding this manuscript. We also thank J. Maisano and T. Rowe for providing us with the HRXCT scan data of *A. leonardi* (FRIM 0026), *A. irregularis* (FMNH 62204), *A. werneri* (FMNH 250439), *C. ruffus* (FMNH 60958); *L. albirostris* (FMNH 216257), *L. dulcis* (TNHC 60638), and *U. melanogaster* (FMNH 167048). These scans were collected as part of the Deep Scaly Project under NSF grant EF-0334961 to M. Kearney and O. Rieppel, and are available on DigiMorph.org. Comparative material from the FMNH, FRIM, UMMZ, USNM, TMM, and TNHC collections were also obtained via DigiMorph. We further thank J. Rosado and J. Hanken of the Harvard Museum of Comparative Zoology for providing access to specimens and permission for CT scanning. Finally, we are grateful to S. Pierce and T. Simões of the Harvard Museum of Comparative Zoology for their assistance in and supervision of the scanning of MCZ specimens. This work was performed in part at the Center for Nanoscale Systems (CNS), a member of the National Nanotechnology Coordinated Infrastructure Network (NNCI), which is supported by the National Science Foundation under NSF award no. 1541959. CNS is part of Harvard University.

For Peer Review Only

Funding was provided via an Alexander Graham Bell Canada Graduate Scholarship awarded by the Natural Sciences and Engineering Research Council of Canada (NSERC) to C.R.C.S. and an NSERC Discovery Grant (#23458) to M.W.C. We have no conflicts of interest to declare.

Author Contributions

C.R.C.S. conducted the micro-CT scanning of MCZ specimens, performed the segmentations and descriptions, and wrote the manuscript. A.P. contributed to drafting the manuscript. M.W.C. conceived of and supervised the project. All authors developed the project and contributed to writing and discussions.

References

Object Research Systems (ORS) Inc. (2019) Dragonfly 4.0. Montreal, Canada. http://www.theobjects.com/dragonfly.

Al-Mohammadi AGA, Khannoon ER, Evans SE (2020) The development of the osteocranium in the snake *Psammophis sibilans* (Serpentes: Lamprophiidae). *J Anat* **236,** 117–131.

Bellairs AD, Underwood G (1951) The origin of snakes. *Biol Rev* **26,** 193–237.

Berkovitz B, Shellis P (2017) *The Teeth of Non-Mammalian Vertebrates*. London: Academic Press.

Boback SM, Dichter EK, Mistry HL (2012) A developmental staging series for the African house snake, *Boaedon* (*Lamprophis*) *fuliginosus*. *Zoology* **115,** 38–46.

Boughner JC, Buchtová M, Fu K, Diewert V, Hallgrímsson B, Richman JM (2007) Embryonic development of *Python sebae* – I: Staging criteria and macroscopic skeletal morphogenesis of the head and limbs. *Zoology* **110,** 212–230.

For Peer Review Only

Caldwell MW (2019) *The Origin of Snakes: Morphology and the Fossil Record.* Boca Raton: Taylor & Francis.

Chretien J, Wang-Claypool CY, Glaw F, Scherz MD (2019) The bizarre skull of *Xenotyphlops* sheds light on synapomorphies of Typhlopoidea. *J Anat* **234,** 637–655.

Cundall D, Rossman DA (1993) Cephalic anatomy of the rare Indonesian snake *Anomochilus weberi*. *Zool J Linn Soc* **109,** 235–273.

Da Silva FO, Fabre A-C, Savriama Y, et al. (2018) The ecological origins of snakes as revealed by skull evolution. *Nature Communications* **9,** 376.

Deufel A, Cundall D (2003) Feeding in *Atractaspis* (Serpentes: Atractaspididae): a study in conflicting functional constraints. *Zoology* **106,** 43–61.

Dong S, Kumazawa Y (2005) Complete mitochondrial DNA sequences of six snakes: phylogenetic relationships and molecular evolution of genomic features. *J Mol Evol* **61,** 12–22.

Evans SE (2008) The Skull of Lizards and Tuatara. In *Biology of the Reptilia, Vol. 20: The skull of Lepidosauria* (eds Gans C, Gaunt AS, Adler K), pp. 1–347. Ithaca: Society for the Study of Amphibians and Reptiles.

Figueroa A, McKelvy AD, Grismer LL, Bell CD, Lailvaux SP (2016) A species-level phylogeny of extant snakes with description of a new colubrid subfamily and genus. *PLoS ONE* **11,** e0161070.

Fröbisch NB, Schoch RR (2009) Testing the impact of miniaturization on phylogeny: Paleozoic dissorophoid amphibians. *Syst Biol* **58,** 312–327.

For Peer Review Only

Garberoglio FF, Apesteguía S, Simões TR, et al. (2019) New skulls and skeletons of the Cretaceous legged snake *Najash*, and the evolution of the modern snake body plan. *Science Advances* **5,** eaax5833.

Gauthier JA, Kearney M, Maisano JA, Rieppel O, Behlke ADB (2012) Assembling the squamate tree of life: Perspectives from the phenotype and the fossil record. *Bull Peabody Mus Nat Hist* **53,** 3–308.

Hanken J (1984) Miniaturization and its effects on cranial morphology in plethodontid salamanders, genus *Thorius* (Amphibia: Plethodontidae). I. Osteological variation. *Biol J Linn Soc* **23,** 55–75.

Hanken J, Wake DB (1993) Miniaturization of body size: organismal consequences and evolutionary significance. *Annu Rev Ecol Syst* **24,** 501–519.

Harrington SM, Reeder TW (2017) Phylogenetic inference and divergence dating of snakes using molecules, morphology and fossils: new insights into convergent evolution of feeding morphology and limb reduction. *Biol J Linn Soc* **121,** 379–394.

Hernández-Jaimes C, Jerez A, Ramírez-Pinilla MP (2012) Embryonic development of the skull of the Andean lizard *Ptychoglossus bicolor* (Squamata, Gymnophthalmidae). *J Anat* **221,** 285–302.

Hsiang AY, Field DJ, Webster TH, et al. (2015) The origin of snakes: revealing the ecology, behavior, and evolutionary history of early snakes using genomics, phenomics, and the fossil record. *BMC Evol Biol* **15,** 87.

Irish FJ (1989) The role of heterochrony in the origin of a novel bauplan: Evolution of the ophidian skull. *Geobios* **22,** 227–233.

For Peer Review Only

Jackson K (2002) Post-ovipositional development of the monocled cobra, *Naja kaouthia* (Serpentes: Elapidae). *Zoology* **105,** 203–214.

Jackson K (2007) The evolution of venom-conducting fangs: Insights from developmental biology. *Toxicon* **49,** 975–981.

Kamal AM (1966) On the process of rotation of the quadrate cartilage in Ophidia. *Anat Anz* **118,** 87–90.

Khannoon ER, Evans SE (2015) The development of the skull of the Egyptian cobra *Naja h. haje* (Squamata: Serpentes: Elapidae). *PLoS ONE* **10,** e0122185.

Khannoon ER, Ollonen J, Di-Poï N (2020) Embryonic development of skull bones in the Sahara horned viper (*Cerastes cerastes*), with new insights into structures related to the basicranium and braincase roof. *J Anat* **00,** 1–19.

Khannoon ER, Zahradnicek O (2017) Postovipositional development ofthe sand snake *Psammophis sibilans* (Serpentes:Lamprophiidae) in comparison with other snake species. *Acta Zool (Stockh)* **98,** 144–153.

Kley NJ (2006) Morphology of the lower jaw and suspensorium in the Texas blindsnake, *Leptotyphlops dulcis* (Scolecophidia: Leptotyphlopidae). *J Morphol* **267,** 494–515.

Kochva E (1987) The origin of snakes and evolution of the venom apparatus. *Toxicon* **25,** 65–106.

Kochva E (2002) *Atractaspis* (Serpentes, Atractaspididae) the burrowing asp; a multidisciplinary minireview. *Bulletin of the Natural History Museum Zoology* **68,** 91–99.

List JC (1966) Comparative osteology of the snake families Typhlopidae and Leptotyphlopidae. *Illinois Biological Monographs* **36,** 1–112.

For Peer Review Only

Longrich NR, Bhullar B-AS, Gauthier JA (2012) A transitional snake from the Late Cretaceous period of North America. *Nature* **488,** 205–208.

Maddin HC, Olori JC, Anderson JS (2011) A redescription of *Carrolla craddocki* (Lepospondyli: Brachystelechidae) based on high-resolution CT, and the impacts of miniaturization and fossoriality on morphology. *J Morphol* **272,** 722–743.

Maisano JA, Rieppel O (2007) The skull of the round island boa, *Casarea dussumieri* Schlegel, based on high-resolution X-ray computed tomography. *J Morphol* **268,** 371–384.

Malmstrøm M, Britz R, Matschiner M, et al. (2018) The most developmentally truncated fishes show extensive *Hox* gene loss and miniaturized genomes. *Genome Biol Evol* **10,** 1088–1103.

McNamara KJ (1986) A guide to the nomenclature of heterochrony. *J Paleontol* **60,** 4–13.

Miralles A, Marin J, Markus D, Herrel A, Hedges SB, Vidal N (2018) Molecular evidence for the paraphyly of Scolecophidia and its evolutionary implications. *J Evol Biol* **31,** 1782–1793.

Mongiardino Koch N, Gauthier JA (2018) Noise and biases in genomic data may underlie radically different hypotheses for the position of Iguania within Squamata. *PLoS ONE* **13,** e0202729.

Moyer K, Jackson K (2011) Phylogenetic relationships among the Stiletto Snakes (genus Atractaspis) based on external morphology. *African Journal of Herpetology* **60,** 30–46.

Olori JC, Bell CJ (2012) Comparative skull morphology of uropeltid snakes (Alethinophidia: Uropeltidae) with special reference to disarticulated elements and variation. *PLoS ONE* **7,** e32450.

For Peer Review Only

Palci A, Caldwell MW (2010) Redescription of *Acteosaurus tommasinii* von Meyer, 1860, and a discussion of evolutionary trends within the clade Ophidiomorpha. *J Vert Paleontol* **30,** 94–108.

Palci A, Caldwell MW (2013) Primary homologies of the circumorbital bones of snakes. *J Morphol* **274,** 973–986.

Palci A, Caldwell MW (2014) The Upper Cretaceous snake *Dinilysia patagonica* Smith-Woodward, 1901, and the crista circumfenestralis of snakes. *J Morphol* **275,** 1187–1200.

Palci A, Hutchinson MN, Caldwell MW, Smith KT, Lee MSY (2020) The homologies and evolutionary reduction of the pelvis and hindlimbs in snakes, with the first report of ossified pelvic vestiges in an anomalepidid (*Liotyphlops beui*). *Zool J Linn Soc* **188,** 630–652.

Palci A, Lee MSY, Hutchinson MN (2016) Patterns of postnatal ontogeny of the skull and lower jaw of snakes as revealed by micro-CT scan data and three-dimensional geometric morphometrics. *J Anat* **229,** 723–754.

Palci A, Seymour RS, Van Nguyen C, Hutchinson MN, Lee MSY, Sanders KL (2019) Novel vascular plexus in the head of a sea snake (Elapidae, Hydrophiinae) revealed by high-resolution computed tomography and histology. *R Soc Open Sci* **6,** 191099.

Polachowski KM, Werneburg I (2013) Late embryos and bony skull development in *Bothropoides jararaca* (Serpentes, Viperidae). *Zoology* **116,** 36–63.

Portillo F, Branch WR, Conradie W, et al. (2018) Phylogeny and biogeography of the African burrowing snake subfamily Aparallactinae (Squamata: Lamprophiidae). *Mol Phylogen Evol* **127,** 288–303.

For Peer Review Only

Portillo F, Stanley EL, Branch WR, et al. (2019) Evolutionary history of burrowing asps (Lamprophiidae: Atractaspidinae) with emphasis on fang evolution and prey selection. *PloS ONE* **14,** e0214889.

Pringle JA (1954) The cranial development of certain South African snakes and the relationship of these groups. *Proc Zool Soc Lond* **123,** 813–865.

Racca L, Villa A, Wencker LCM, Camaiti M, Blain H-A, Delfino M (2020) Skull osteology and osteological phylogeny of the Western whip snake *Hierophis viridiflavus* (Squamata, Colubridae). *J Morphol* **281,** 808–833.

Reeder TW, Townsend TM, Mulcahy DG, et al. (2015) Integrated analyses resolve conflicts over squamate reptile phylogeny and reveal unexpected placements for fossil taxa. *PLoS ONE* **10,** e0118199.

Reinhardt JT (1843) Beskrivelse af nogle nye Slangearter. *Kongel Dansk Vidensk Selsk Afhandl* **10,** 233–279.

Rieppel O (1978) The evolution of the naso-frontal joint in snakes and its bearing on snake origins. *J Zool Syst Evol Res* **16,** 14–27.

Rieppel O (1979) The evolution of the basicranium in the Henophidia (Reptilia: Serpentes). *Zool J Linn Soc* **66,** 411–431.

Rieppel O (1988) A review of the origin of snakes. In *Evolutionary Biology* (eds Hecht MK, Wallace B, Prance GT), pp. 37–130. Boston, MA: Springer.

Rieppel O (1996) Miniaturization in tetrapods: consequences for skull morphology. In *Miniature Vertebrates: The Implications of Small Body Size, Vol. 69. Symposia of the Zoological Society of London* (ed Miller PJ), pp. 47–61. Oxford: Claredon Press.

For Peer Review Only

Rieppel O (2007) The naso-frontal joint in snakes as revealed by high-resolution X-ray computed tomography of intact and complete skulls. *Zool Anz* **246,** 177–191.

Rieppel O (2012) "Regressed" macrostomatan snakes. *Fieldiana Life and Earth Sciences* **2012,** 99–103.

Rieppel O, Kley NJ, Maisano JA (2009) Morphology of the skull of the white-nosed blindsnake, *Liotyphlops albirostris* (Scolecophidia: Anomalepididae). *J Morphol* **270,** 536–557.

Rieppel O, Maisano JA (2007) The skull of the rare Malaysian snake *Anomochilus leonardi* Smith, based on high-resolution X-ray computed tomography. *Zool J Linn Soc* **149,** 671–685.

Rieppel O, Zaher H (2000) The intramandibular joint in squamates, and the phylogenetic relationships of the fossil snake *Pachyrhachis problematicus* Haas. *Fieldiana Geology* **43,** 1–69.

Rieppel O, Zaher H (2001) The development of the skull in *Acrochordus granulatus* (Schneider) (Reptilia: Serpentes), with special consideration of the otico-occipital complex. *J Morphol* **249,** 252–266.

Rödel M-O, Kucharzewski C, Mahlow K, et al. (2019) A new stiletto snake (Lamprophiidae, Atractaspidinae, Atractaspis) from Liberia and Guinea, West Africa. *Zoosystematics and Evolution* **95,** 107–123.

Savitzky AH (1983) Coadapted character complexes among snakes: Fossoriality, piscivory, and durophagy. *Am Zool* **23,** 397–409.

Scanferla A (2016) Postnatal ontogeny and the evolution of macrostomy in snakes. *R Soc Open Sci* **3,** 160612.

For Peer Review Only

Scanferla A, Bhullar B-AS (2014) Postnatal development of the skull of *Dinilysia patagonica* (Squamata-Stem Serpentes). *The Anatomical Record* **297,** 560–573.

Sherratt E, Sanders KL, Watson A, Hutchinson MN, Lee MSY, Palci A (2019) Heterochronic shifts mediate ecomorphological convergence in skull shape of microcephalic sea snakes. *Integr Comp Biol* **59,** 616–624.

Sheverdyukova HV (2017) Development of the osteocranium in *Natrix natrix* (Serpentes, Colubridae) embryogenesis I: development of cranial base and cranial vault. *Zoomorphology* **136,** 131–143.

Sheverdyukova HV (2019) Development of the osteocranium in *Natrix natrix* (Serpentes, Colubridae) embryogenesis II: development of the jaws, palatal complex and associated bones. *Acta Zool* **100,** 282–291.

Sheverdyukova HV, Kovtun MF (2020) Variation in the formation of crista sellaris and basisphenoid in the skull of the grass snake *Natrix natrix* embryos (Serpentes, Colubridae). *J Morphol* **281,** 338–347.

Shine R, Branch WR, Harlow PS, Webb JK, Shine T (2006) Biology of burrowing asps (Atractaspididae) from Southern Africa. *Copeia* **1,** 103–115.

Simões TR, Caldwell MW, Tałanda M, et al. (2018) The origin of squamates revealed by a Middle Triassic lizard from the Italian Alps. *Nature* **557,** 706–709.

Strong CRC, Simões TR, Caldwell MW, Doschak MR (2019) Cranial ontogeny of *Thamnophis radix* (Serpentes: Colubroidea) with a re-evaluation of current paradigms of snake skull evolution. *R Soc Open Sci* **6,** 182228.

Struck TH (2007) Data congruence, paedomorphosis and salamanders. *Frontiers in Zoology* **4,** 22.

For Peer Review Only

Underwood G, Kochva E (1993) On the affinities of the burrowing asps *Atractaspis* (Serpentes: Atractaspididae). *Zool J Linn Soc* **107,** 3–64.

Vidal N, Branch WR, Pauwels OSG, et al. (2008) Dissecting the major African snake radiation: A molecular phylogeny of the Lamprophiidae Fitzinger (Serpentes, Caenophidia). *Zootaxa* **1945,** 51–66.

Wake MH (1986) The morphology of *ldiocranium russeli* (Amphibia: Gymnophiona), with comments on miniaturization through heterochrony. *J Morphol* **189,** 1–16.

Wake MH (1993) The Skull as a Locomotor Organ. In *The Skull: Functional and Evolutionary Mechanisms* (eds Hanken J, Hall BK), pp. 216. Chicago: University of Chicago Press.

Walls GL (1942) The vertebrate eye and its adaptive radiation. *Bulletin of the Cranbrook Institute of Science* **19,** 1–785.

Werneburg I, Sánchez-Villagra MR (2015) Skeletal heterochrony is associated with the anatomical specializations of snakes among squamate reptiles. *Evolution* **69,** 254–263.

Wiens JJ, Bonett RM, Chippindale PT (2005) Ontogeny discombobulates phylogeny: Paedomorphosis and higher-level salamander relationships. *Syst Biol* **54,** 91–110.

Yan J, Li H, Zhou K (2008) Evolution of the mitochondrial genome in snakes: gene rearrangements and phylogenetic relationships. *BMC Genomics* **9,** 569.

Young BA (1987) The cranial nerves of three species of sea snakes. *Can J Zool/Rev Can Zool* **65,** 2236–2240.

Young BA (1989) Ontogenetic changes in the feeding system of the red-sided garter snake, *Thamnophis sirtalis parietalis*. I. Allometric analysis. *J Zool* **218,** 365–381.

Zaher H, Grazziotin FG, Cadle JE, Murphy RW, Moura-Leite JCd, Bonatto SL (2009) Molecular phylogeny of advanced snakes (Serpentes, Caenophidia) with an emphasis on

For Peer Review Only

South American Xenodontines: a revised classification and descriptions of new taxa. *Pap Avuls Zool* **49,** 115–153.

Zaher H, Murphy RW, Arredondo JC, et al. (2019) Large-scale molecular phylogeny, morphology, divergence-time estimation, and the fossil record of advanced caenophidian snakes (Squamata: Serpentes). *PLoS ONE* **14,** e0216148.

Zehr DR (1962) Stages in the normal development of the Common Garter Snake, *Thamnophis sirtalis sirtalis*. *Copeia* **1962,** 322–329.

Zheng Y, Wiens JJ (2016) Combining phylogenomic and supermatrix approaches, and a time-calibrated phylogeny for squamate reptiles (lizards and snakes) based on 52 genes and 4162 species. *Mol Phylogen Evol* **94,** 537–547.

Supplementary Material

The data supporting the results of this study are available in the Supporting Information section.

Figs S1–S23. Surface meshes of each skull element of *Atractaspis irregularis* (FMNH 62204), embedded in 3D PDFs. To view each mesh, open the file in Adobe Acrobat and click on the model to activate it. Further imagery of this specimen is available on DigiMorph.org (http://digimorph.org/specimens/Atractaspis_irregularis/).

S24. Complete HRXCT scan parameters.

S25. Overview of skeletal pathologies of FMNH 62204.

Figure Legends

Figure 1. Skull of *Atractaspis irregularis* (FMNH 62204) in (A) lateral view (right lateral, reflected), (B) dorsal view, (C) ventral view with mandibles, and (D) ventral view with

For Peer Review Only

mandibles removed. Colouration of bones is consistent throughout all panels. Surface mesh files of each element are available as 3D PDFs in the Supporting Information (Figs S1–S23). Abbreviations: ang, angular; bo, basioccipital; cb, compound bone; d, dentary; ecp, ectopterygoid; f, frontal; mx, maxilla; n, nasal; oto, otoccipital; p, parietal; pal, palatine; pbs, parabasisphenoid; pf, prefrontal; pmx, premaxilla; pro, prootic; pt, pterygoid; q, quadrate; smx, septomaxilla; so, supraoccipital; spl, splenial; st, supratemporal; v, vomer.

Figure 2. Snout unit and elements of *Atractaspis irregularis* (FMNH 62204). (A) Snout in articulation with the skull (right lateral view, reflected). (B–D) Articulated snout elements in (B) lateral, (C) anterior, and (D) dorsal views. (E–H) Premaxilla in (E) lateral, (F) anterior, (G) dorsal, and (H) posterior views. (I–L) Left septomaxilla in (I**)** lateral, (J) medial, (K) dorsal, and (L) ventral views. (M–R) Left vomer in (M) lateral, (N) medial, (O) dorsal, (P) ventral, (Q) anterior, and (R) posterior views. (S–U) Nasals in (S) dorsal, (T) lateral, and (U) ventral views. Upper scale bar applies to (A); lower scale bar applies to (B–U). Colouration of bones is consistent throughout all panels. Arrows beneath panel labels point anteriorly. Surface mesh files of each element are available as 3D PDFs in the Supporting Information (Figs S1–S23). Abbreviations: a.Smx, articulatory surface for the septomaxilla; dl.N, dorsal lamina of the nasal; fv, fenestra vomeronasalis; lal, lateral ascending lamina; mal, medial ascending lamina; mnf, medial nasal flange; n, nasal; np.Pmx, nasal process of the premaxilla; pmx, premaxilla; plp, palatal process; pmp, premaxillary process; pmxf, premaxillary foramen; pp.Smx, posterior process of the septomaxilla; smx, septomaxilla; tp, transverse process; v, vomer; vc.Smx, vomeronasal cupola of the septomaxilla; vc.V, vomeronasal cupola of the vomer; vp, vomerine process.

For Peer Review Only

Figure 3. Skull roof of *Atractaspis irregularis* (FMNH 62204). (A) Skull roof in articulation with the skull (dorsal view). (B–D) Parietal in (B) lateral, (C) ventral, and (D) anterior views. (E–H) Frontal in (E) lateral, (F) ventral, (G) anterior, and (H) posterior views. Upper scale bar applies to (A); lower scale bar applies to (B–H). Colouration of bones is consistent throughout all panels. Arrows beneath panel labels point anteriorly. Surface mesh files of each element are available as 3D PDFs in the Supporting Information (Figs S1–S23). Abbreviations: a.Pf, articulatory surface for the prefrontal; a.Psr, articulatory surface for the parasphenoid rostrum; df.F, descending flange of the frontal; f, frontal; mfp, medial frontal pillar; of, optic foramen; ot, olfactory tract; p, parietal; pvp, posteroventral process; sop, subolfactory process.

Figure 4. Palatomaxillary complex of *Atractaspis irregularis* (FMNH 62204). (A) Palatomaxillary complex in articulation with the skull (right lateral view). (B–C) Articulated left palatomaxillary elements in (B) dorsal and (C) medial views. Colouration of bones is consistent throughout all panels. Arrows beneath panel labels point anteriorly. Surface mesh files of each element are available as 3D PDFs in the Supporting Information (Figs S1–S23). Abbreviations: ecp, ectopterygoid; mx, maxilla; pal, palatine; pf, prefrontal; pt, pterygoid.

Figure 5. Palatomaxillary elements of *Atractaspis irregularis* (FMNH 62204). (A–D) Left pterygoid in (A) lateral, (B) medial, (C) dorsal, and (D) ventral views. (E–F) Left ectopterygoid in (E) dorsal and (F) ventral views. (G–K) Left palatine in (G) lateral, (H) medial, (I) anterior, (J) dorsal, and (K) ventral views. (L–Q) Left prefrontal in (L) lateral, (M) anterior, (N) dorsal, (O) medial, (P) posterior, and (Q) ventral views. (R–U) Right maxilla in (R) lateral, (S) medial, (T) dorsal, and (U) ventral views. Colouration of bones is consistent with other figures. Arrows beneath panel labels point anteriorly. Surface mesh files of each element are available as 3D PDFs in the Supporting Information (Figs S1–S23). Abbreviations: a.Ecp, articulatory surface

For Peer Review Only

for the ectopterygoid; a.F, articulatory surface for the frontal; a.Mx, articulatory surface for the maxilla; a.Pf, articulatory surface for the prefrontal; b.Pal, main body of the palatine; cp, choanal process; dl.Pf, dorsal lappet of the prefrontal; ld, lacrimal duct; mp.Ecp, maxillary process of the ectopterygoid; mp.Pal, maxillary process of the palatine; pp.Ecp, pterygoid process of the ectopterygoid; sac, superior alveolar canal; t, tooth; t,f, functional tooth; t.r, replacement tooth; t.s, tooth socket; vch, venom channel.

Figure 6. Braincase unit and constituent elements of *Atractaspis irregularis* (FMNH 62204). (A) Braincase in articulation with the skull (right lateral view). (B–C) Articulated braincase elements in (B) medial and (C) lateral views. (D–F) Parabasisphenoid in (D) dorsal, (E) ventral, and (F) anterodorsal views. (G–H) Basioccipital in (G) dorsal and (H) ventral views. Panels B and C not to scale. Colouration of bones is consistent throughout all panels. Arrows beneath panel labels point anteriorly. Surface mesh files of each element are available as 3D PDFs in the Supporting Information (Figs S1–S23). Abbreviations: bp, basipterygoid process; b.Pbs, main body of the parabasisphenoid; bo, basioccipital; bt, basioccipital tubercle; icf, internal carotid foramen; ls, laterosphenoid ossification; oc, occipital condyle; oto, otoccipital; pao.vc, primary anterior opening of the Vidian canal; po.vc, posterior opening of the Vidian canal; pbs, parabasisphenoid; pro, prootic; psr, parasphenoid rostrum; s, stapes; sao.vc, secondary anterior opening of the Vidian canal; sel, sella turcica; so, supraoccipital.

Figure 7. Braincase elements of *Atractaspis irregularis* (FMNH 62204). (A–D) Right prootic in (A) lateral, (B) medial, (C) anterior, and (D) posterior views. (E–G) Supraoccipital in (E) dorsal, (F) ventral, and (G) left lateral views. (H–L) Right otoccipital in (H) lateral, (I) medial, (J) anterior, (K) posterior, and (L) right posterolateral views. (M–O) Right stapes in (M) posterior, (N) lateral, and (O) medial views. Colouration of bones is consistent with other figures. Arrows

For Peer Review Only

beneath panel labels point anteriorly. Surface mesh files of each element are available as 3D PDFs in the Supporting Information (Figs S1–S23). Abbreviations: asc, anterior semicircular canal; a.St, articulatory surface for the supratemporal; cso, circumstapedial openings; ct, crista tuberalis; dp, descending process; ef, endolymphatic foramen; f.hbVII, foramen for the hyomandibular branch of the facial nerve (CN VII); fo, fenestra ovalis; f.pbVII, foramen for the palatine branch of the facial nerve (CN VII); f.tfc, foramen for the trigemino-facialis chamber; f.VII, foramen for the facial nerve (CN VII); f.VIII, foramen for the acoustic nerve (CN VIII); f.XII, foramen for the hypoglossal nerve (CN XII); hsc, horizontal semicircular canal; io.f.pbVII, internal opening of the foramen for the palatine branch of the facial nerve (CN VII); io.jf, internal opening of the jugular foramen; jf, jugular foramen; jxr, juxtastapedial recess; lf, laterosphenoid foramen; ls, laterosphenoid ossification; marst, medial aperture of the recessus scalae tympani, oc, occipital condyle; otc, otic capsule; psc, posterior semicircular canal; scr, sagittal crest; sf, stapedial footplate; ss, stapedial shaft; V2, foramen for the maxillary (V2) branch of the trigeminal nerve (CN V); V3, foramen for the mandibular (V3) branch of the trigeminal nerve (CN V).

Figure 8. Suspensorium and mandible of *Atractaspis irregularis* (FMNH 62204). (A) Suspensorium and mandible in articulation with the skull (right lateral view). (B) Articulated right mandible in medial view. Colouration of bones is consistent throughout all panels. Arrows beneath panel labels point anteriorly. Surface mesh files of each element are available as 3D PDFs in the Supporting Information (Figs S1–S23). Abbreviations: ang, angular; cb, compound bone; d, dentary; q, quadrate; spl, splenial; st, supratemporal.

Figure 9. Suspensorial and mandibular elements of *Atractaspis irregularis* (FMNH 62204). (A–B) Right quadrate in (A) lateral and (B) medial views. (C–D) Right dentary in (C) dorsal and (D)

For Peer Review Only

medial views. (E–G) Left compound bone in (E) lateral, (F) medial, and (G) dorsal views. (H–J) Right compound bone in (H) lateral, (I) medial, and (J) dorsal views. (K–L) Right supratemporal in (K) lateral and (L) medial views. (M–N) Right angular in (M) lateral and (N) medial views. (O–P) Right splenial in (O) lateral and (P) medial views. Both left and right compound bones are depicted due to likely pathologic alteration posteriorly on the left counterpart and breakage anteriorly on the right counterpart. Colouration of bones is consistent with other figures. Arrows beneath panel labels point anteriorly. Surface mesh files of each element are available as 3D PDFs in the Supporting Information (Figs S1–S23). Abbreviations: a.Br, articulatory surface for the braincase; a.Cb, articulatory surface for the compound bone; a.D, articulatory surface for the dentary; amf, anterior mylohyoid foramen; ap.S, articulatory process for the stapes; a.Q, articulatory surface for the quadrate; a.St, articulatory surface for the supratemporal; f.ctbVII, foramen for the chorda tympani branch of the facial nerve (CN VII); mcan, Meckelian canal; mc.Cb, mandibular condyle of the compound bone; mc.Q, mandibular condyle of the quadrate; mf, mandibular fossa; pmf, posterior mylohyoid foramen.

Figure 10. Morphology of the naso-frontal joint in select fossorial snakes. Each panel shows a cross-section of the frontal and a dorsal view of the skull. Dashed lines represent transmission of force while burrowing, as described by Cundall and Rossman (1993) and Rieppel et al. (2009). Key taxa are indicated in bold. (A) *Atractaspis irregularis* (FMNH 62204), exemplifying the 'central rod design' of the skull in fossorial snakes. (B) *Aparallactus werneri* (FMNH 250439), representing a mixture of the 'central rod' and 'outer shell' designs in an atractaspidid snake. (C) *Anomochilus leonardi* (FRIM 0026), representing a mixture of the 'central rod' and 'outer shell' designs in an alethinophidian snake. (D) *Leptotyphlops dulcis* (UAMZ R335), representing a mixture of the 'central rod' and 'outer shell' designs in a scolecophidian snake. (E) *Indotyphlops*

For Peer Review Only

braminus (UAMZ R363), exemplifying the 'outer shell design' of the skull. Phylogeny from the combined-data analysis of Hsiang et al. (2015). Specimens not to scale.

Figure 11. 'Regressed alethinophidian' hypothesis of scolecophidian evolution. (A) Example of how 'regression' from a 'typical' or non-fossorial alethinophidian skull (represented by the colubroid *Thamnophis radix*, UAMZ R636), to a fossorial alethinophidian (represented by *Atractaspis irregularis*, FMNH 62204), to a typhlopoid skull morphology (*Indotyphlops braminus*, UAMZ R363) could easily occur due to fossorial adaptations, paedomorphosis, and miniaturization. (B) Example of how the leptotyphlopid skull (*Leptotyphlops dulcis*, TNHC 60638) could easily be derived from that of a basal alethinophidian (*Cylindrophis ruffus*, FMNH 60958) through accumulation of fossorial adaptations, paedomorphosis, and miniaturization. In this scenario, *Anomochilus leonardi* (FRIM 0026) would represent an ideal morphological intermediate between the two endpoint skull types. We propose that miniaturization in scolecophidians further superimposes unique features overtop an ancestral fossorial alethinophidian morphotype. Note that these are only examples of morphological grades and do not imply phylogenetic relationships, only that the scolecophidian skull typology could be derived from an ancestral alethinophidian condition. Elements of the jaws and suspensorium affected by paedomorphosis are highlighted. Colouration of bones is consistent throughout panels. Specimens not to scale. Abbreviations: cb, compound bone; d, dentary; ecp, ectopterygoid; mx, maxilla; pal, palatine; pt, pterygoid; q, quadrate; st, supratemporal.

Figure 12. Competing hypotheses of scolecophidian evolution. (A) Traditional phylogeny of extant snakes (Serpentes), in which scolecophidians are the earliest-diverging lineage. (B) Recent phylogeny recovering scolecophidians as 'regressed alethinophidians', i.e., descended from an alethinophidian ancestor. Key groups are indicated in bold. Quotation marks indicate

For Peer Review Only

paraphyletic groups. Topologies in (A) and (B) are adapted from Rieppel (1988) and Garberoglio et al. (2019), respectively.

For Peer Review Only

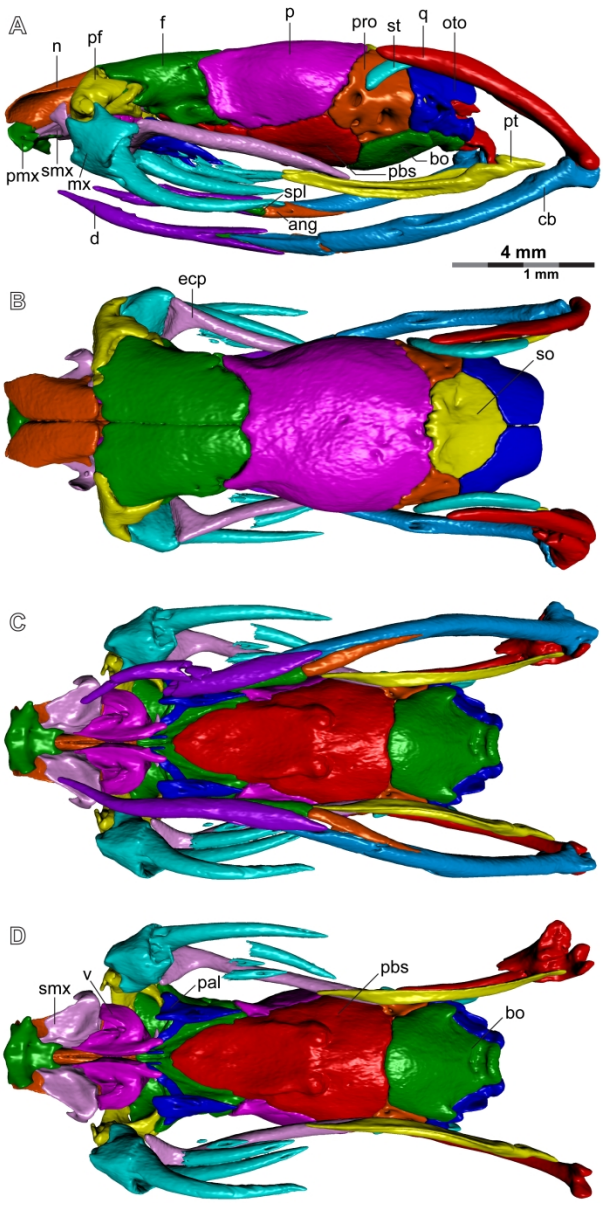

Figure 1. Skull of *Atractaspis irregularis* (FMNH 62204) in (A) lateral view (right lateral, reflected), (B) dorsal view, (C) ventral view with mandibles, and (D) ventral view with mandibles removed. Colouration of bones is consistent throughout all panels. Surface mesh files of each element are available as 3D PDFs in the Supporting Information (Figs S1–S23). Abbreviations: ang, angular; bo, basioccipital; cb, compound bone; d, dentary; ecp, ectopterygoid; f, frontal; mx, maxilla; n, nasal; oto, otoccipital; p, parietal; pal, palatine; pbs, parabasisphenoid; pf, prefrontal; pmx, premaxilla; pro, prootic; pt, pterygoid; q, quadrate; smx, septomaxilla; so, supraoccipital; spl, splenial; st, supratemporal; v, vomer.

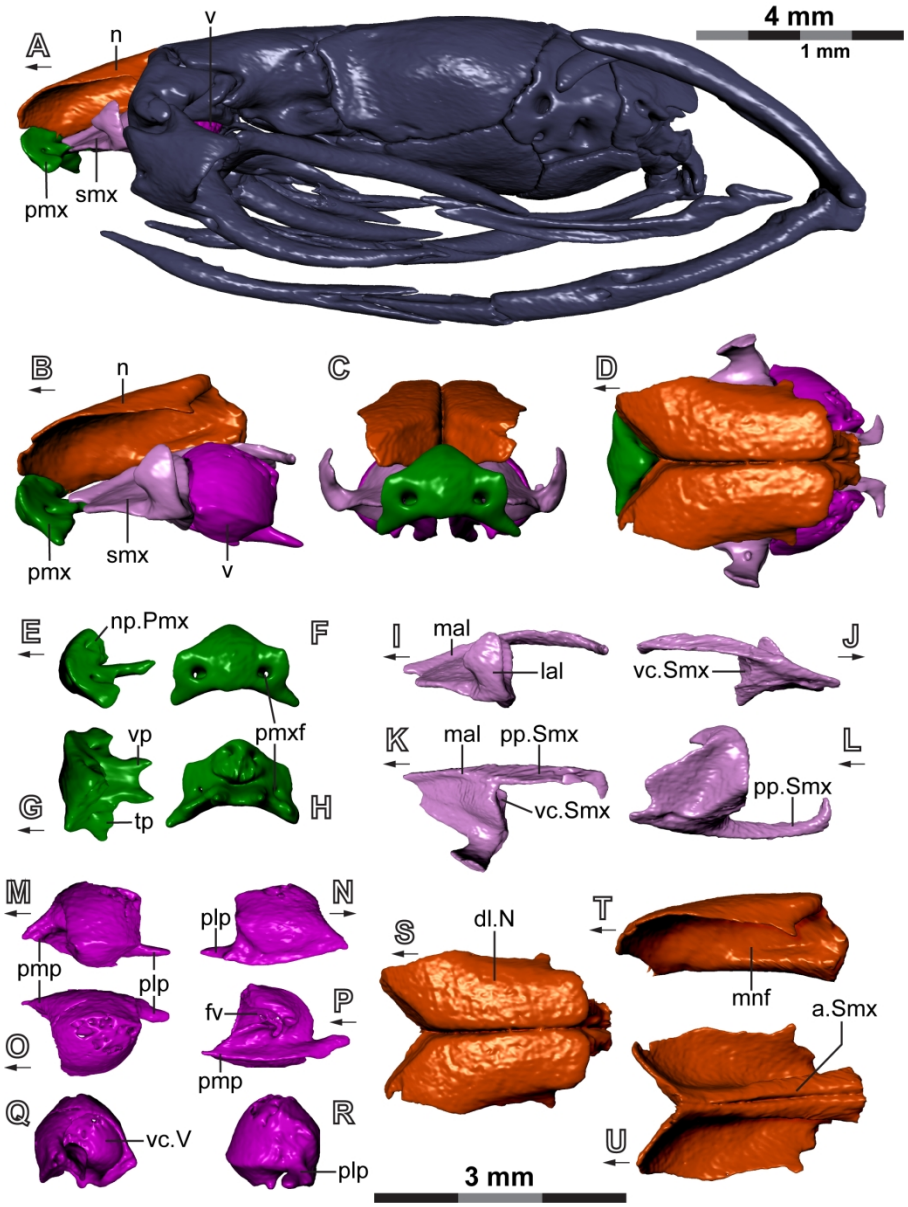

Figure 2. Snout unit and elements of *Atractaspis irregularis* (FMNH 62204). (A) Snout in articulation with the skull (right lateral view, reflected). (B–D) Articulated snout elements in (B) lateral, (C) anterior, and (D) dorsal views. (E–H) Premaxilla in (E) lateral, (F) anterior, (G) dorsal, and (H) posterior views. (I–L) Left septomaxilla in (I) lateral, (J) medial, (K) dorsal, and (L) ventral views. (M–R) Left vomer in (M) lateral, (N) medial, (O) dorsal, (P) ventral, (Q) anterior, and (R) posterior views. (S–U) Nasals in (S) dorsal, (T) lateral, and (U) ventral views. Upper scale bar applies to (A); lower scale bar applies to (B–U). Colouration of bones is consistent throughout all panels. Arrows beneath panel labels point anteriorly. Surface mesh files of each element are available as 3D PDFs in the Supporting Information (Figs S1–S23). Abbreviations: a.Smx, articulatory surface for the septomaxilla; dl.N, dorsal lamina of the nasal; fv, fenestra vomeronasalis; lal, lateral ascending lamina; mal, medial ascending lamina; mnf, medial nasal flange; n, nasal; np.Pmx, nasal process of the premaxilla; pmx, premaxilla; plp, palatal process; pmp, premaxillary process; pmxf, premaxillary foramen; pp.Smx, posterior process of the septomaxilla; smx, septomaxilla; tp, transverse process; v, vomer; vc.Smx, vomeronasal cupola of the septomaxilla; vc.V, vomeronasal cupola of the vomer; vp, vomerine process.

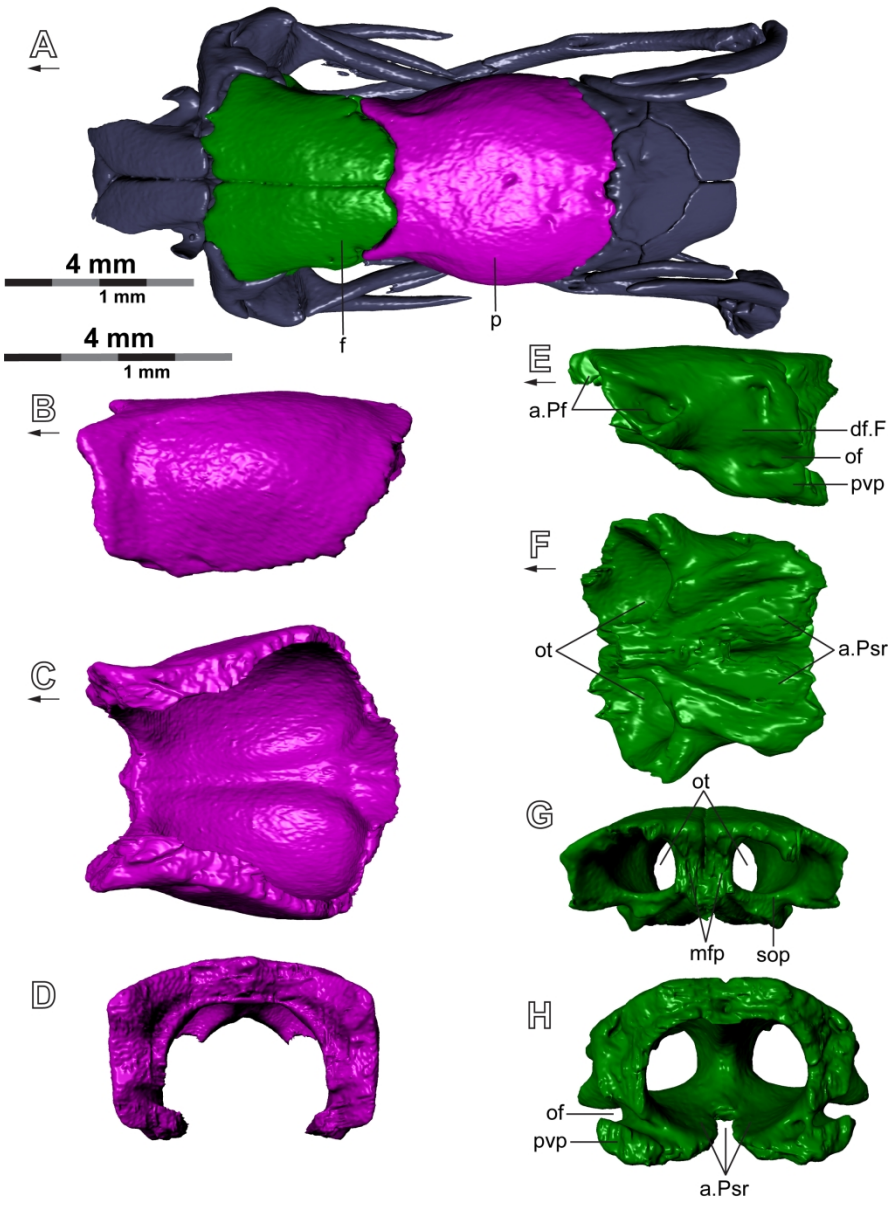

Figure 3. Skull roof of *Atractaspis irregularis* (FMNH 62204). (A) Skull roof in articulation with the skull (dorsal view). (B–D) Parietal in (B) lateral, (C) ventral, and (D) anterior views. (E–H) Frontal in (E) lateral, (F) ventral, (G) anterior, and (H) posterior views. Upper scale bar applies to (A); lower scale bar applies to (B–H). Colouration of bones is consistent throughout all panels. Arrows beneath panel labels point anteriorly. Surface mesh files of each element are available as 3D PDFs in the Supporting Information (Figs S1–S23). Abbreviations: a.Pf, articulatory surface for the prefrontal; a.Psr, articulatory surface for the parasphenoid rostrum; df.F, descending flange of the frontal; f, frontal; mfp, medial frontal pillar; of, optic foramen; ot, olfactory tract; p, parietal; pvp, posteroventral process; sop, subolfactory process.

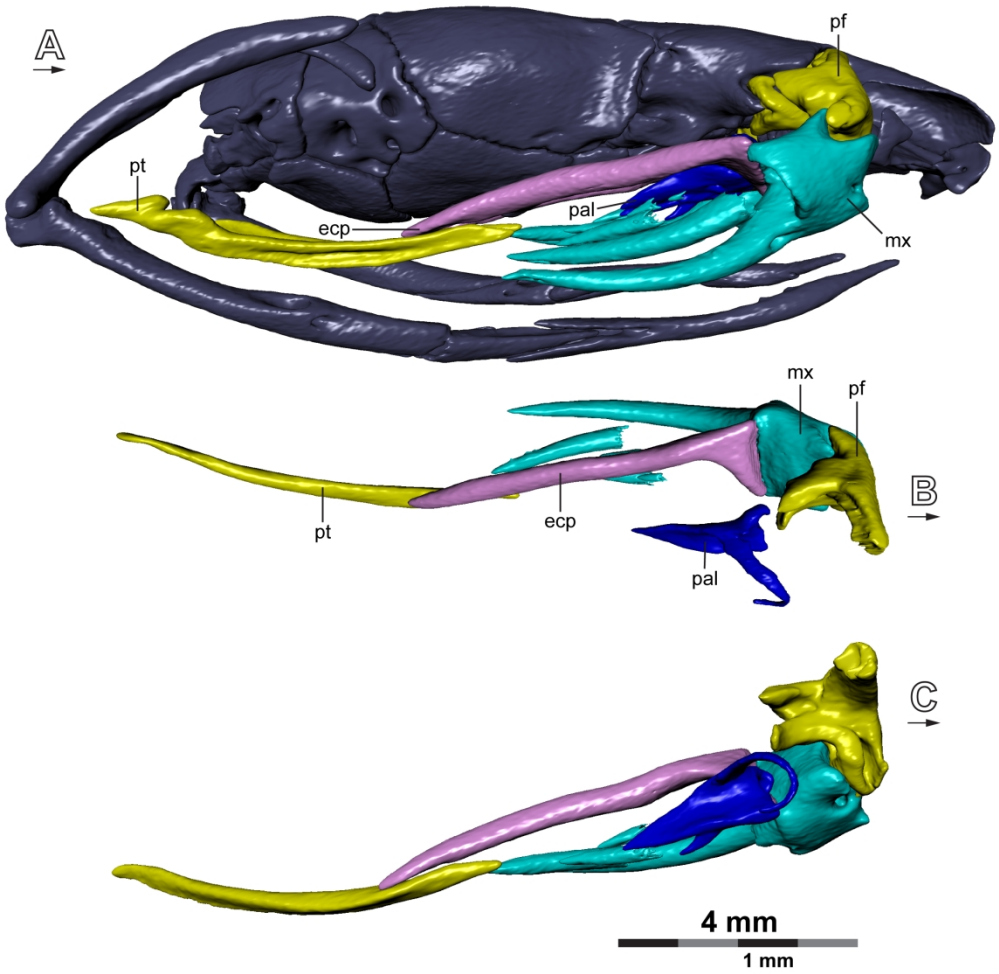

Figure 4. Palatomaxillary complex of *Atractaspis irregularis* (FMNH 62204). (A) Palatomaxillary complex in articulation with the skull (right lateral view). (B–C) Articulated left palatomaxillary elements in (B) dorsal and (C) medial views. Colouration of bones is consistent throughout all panels. Arrows beneath panel labels point anteriorly. Surface mesh files of each element are available as 3D PDFs in the Supporting Information (Figs S1–S23). Abbreviations: ecp, ectopterygoid; mx, maxilla; pal, palatine; pf, prefrontal; pt, pterygoid.

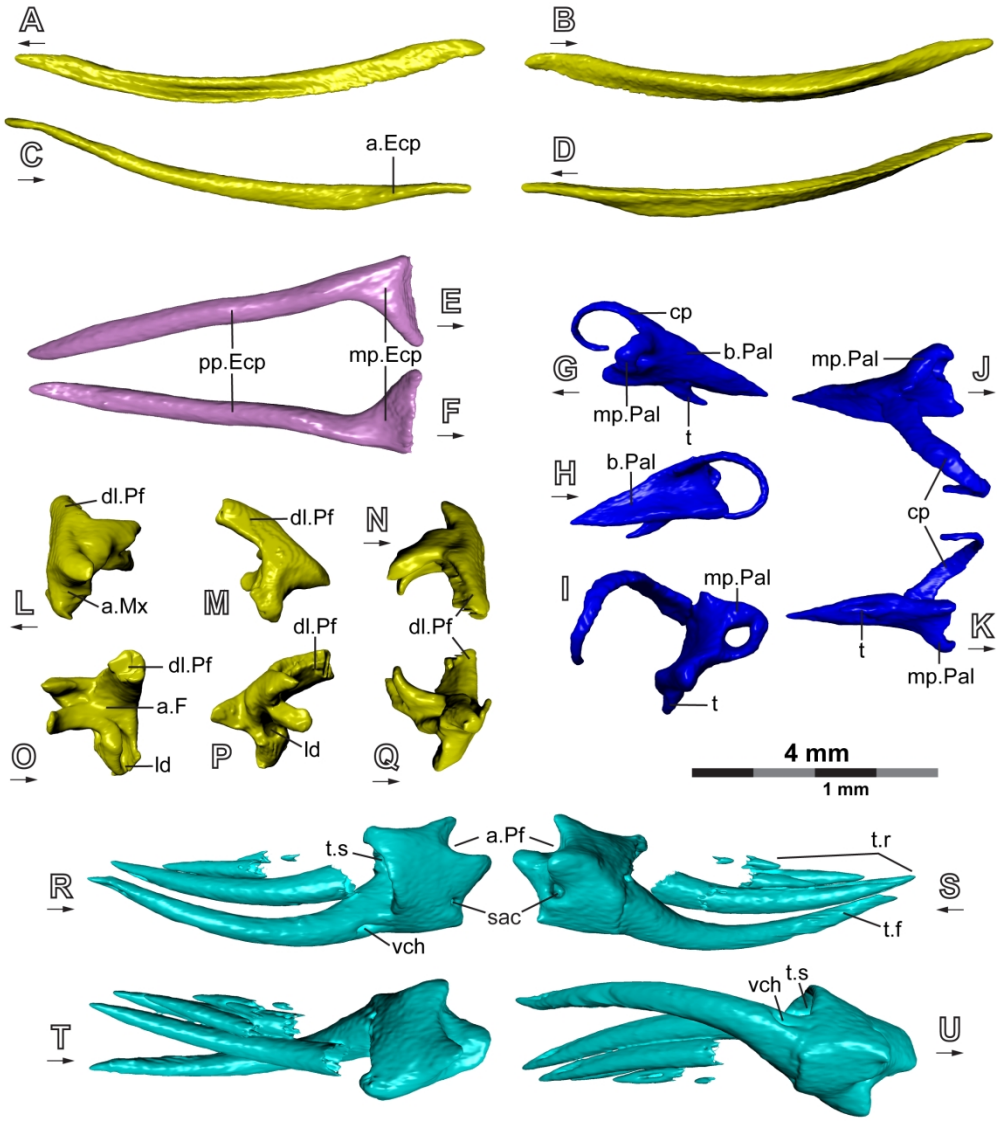

Figure 5. Palatomaxillary elements of *Atractaspis irregularis* (FMNH 62204). (A–D) Left pterygoid in (A) lateral, (B) medial, (C) dorsal, and (D) ventral views. (E–F) Left ectopterygoid in (E) dorsal and (F) ventral views. (G–K) Left palatine in (G) lateral, (H) medial, (I) anterior, (J) dorsal, and (K) ventral views. (L–Q) Left prefrontal in (L) lateral, (M) anterior, (N) dorsal, (O) medial, (P) posterior, and (Q) ventral views. (R–U) Right maxilla in (R) lateral, (S) medial, (T) dorsal, and (U) ventral views. Colouration of bones is consistent with other figures. Arrows beneath panel labels point anteriorly. Surface mesh files of each element are available as 3D PDFs in the Supporting Information (Figs S1–S23). Abbreviations: a.Ecp, articulatory surface for the ectopterygoid; a.F, articulatory surface for the frontal; a.Mx, articulatory surface for the maxilla; a.Pf, articulatory surface for the prefrontal; b.Pal, main body of the palatine; cp, choanal process; dl.Pf, dorsal lappet of the prefrontal; ld, lacrimal duct; mp.Ecp, maxillary process of the ectopterygoid; mp.Pal, maxillary process of the palatine; pp.Ecp, pterygoid process of the ectopterygoid; sac, superior alveolar canal; t, tooth; t,f, functional tooth; t.r, replacement tooth; t.s, tooth socket; vch, venom channel.

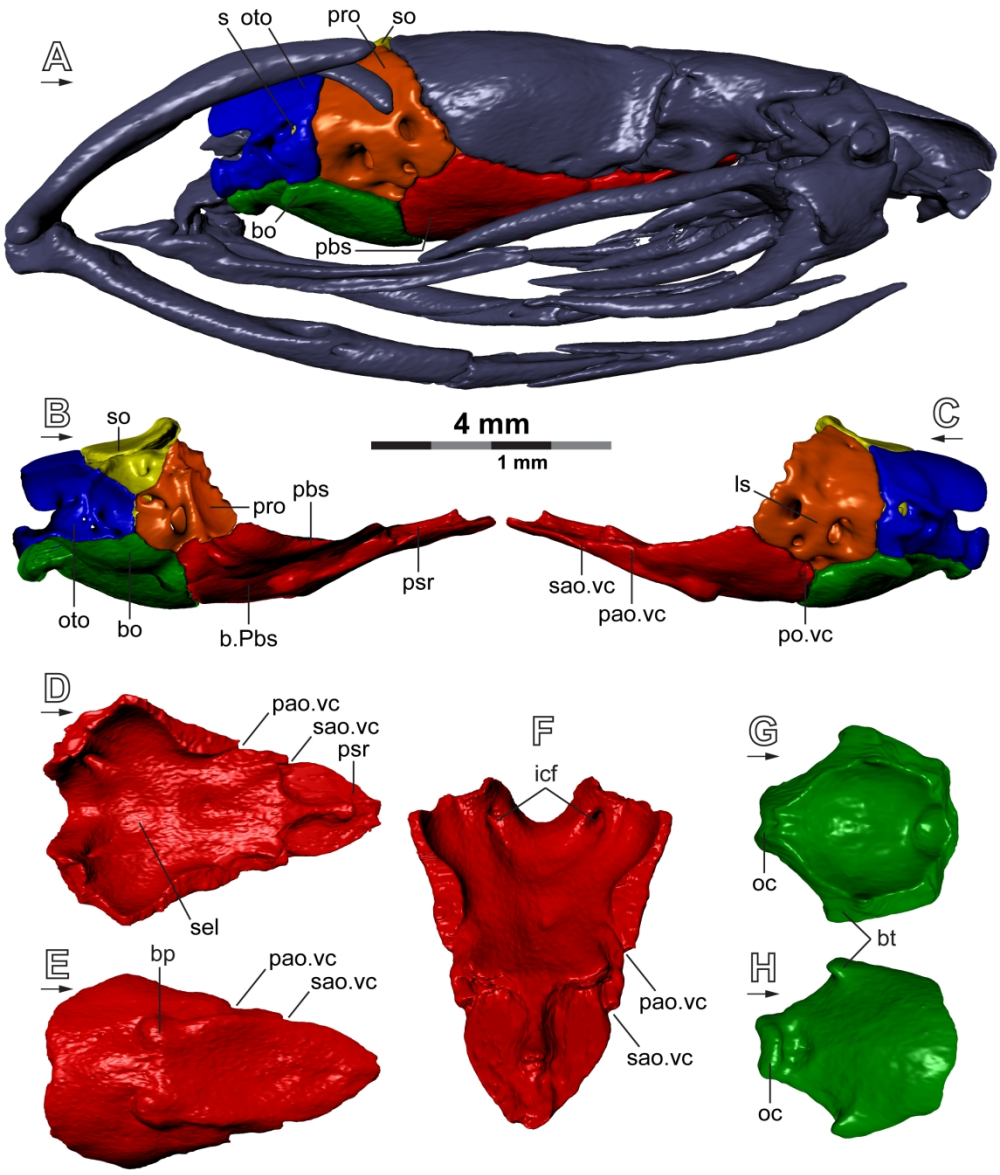

Figure 6. Braincase unit and constituent elements of *Atractaspis irregularis* (FMNH 62204). (A) Braincase in articulation with the skull (right lateral view). (B–C) Articulated braincase elements in (B) medial and (C) lateral views. (D–F) Parabasisphenoid in (D) dorsal, (E) ventral, and (F) anterodorsal views. (G–H) Basioccipital in (G) dorsal and (H) ventral views. Panels B and C not to scale. Colouration of bones is consistent throughout all panels. Arrows beneath panel labels point anteriorly. Surface mesh files of each element are available as 3D PDFs in the Supporting Information (Figs S1–S23). Abbreviations: bp, basipterygoid process; b.Pbs, main body of the parabasisphenoid; bo, basioccipital; bt, basioccipital tubercle; icf, internal carotid foramen; ls, laterosphenoid ossification; oc, occipital condyle; oto, otoccipital; pao.vc, primary anterior opening of the Vidian canal; po.vc, posterior opening of the Vidian canal; pbs, parabasisphenoid; pro, prootic; psr, parasphenoid rostrum; s, stapes; sao.vc, secondary anterior opening of the Vidian canal; sel, sella turcica; so, supraoccipital.

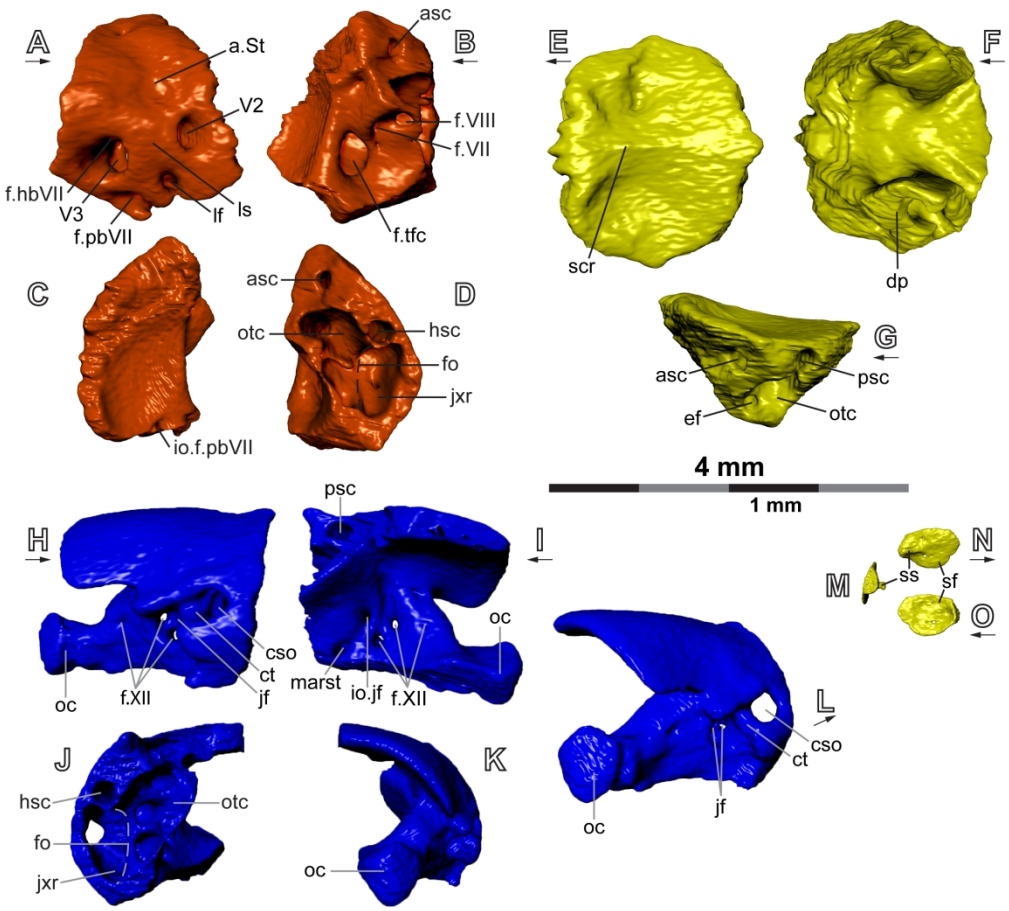

Figure 7. Braincase elements of *Atractaspis irregularis* (FMNH 62204). (A–D) Right prootic in (A) lateral, (B) medial, (C) anterior, and (D) posterior views. (E–G) Supraoccipital in (E) dorsal, (F) ventral, and (G) left lateral views. (H–L) Right otoccipital in (H) lateral, (I) medial, (J) anterior, (K) posterior, and (L) right posterolateral views. (M–O) Right stapes in (M) posterior, (N) lateral, and (O) medial views. Colouration of bones is consistent with other figures. Arrows beneath panel labels point anteriorly. Surface mesh files of each element are available as 3D PDFs in the Supporting Information (Figs S1–S23). Abbreviations: asc, anterior semicircular canal; a.St, articulatory surface for the supratemporal; cso, circumstapedial openings; ct, crista tuberalis; dp, descending process; ef, endolymphatic foramen; f.hbVII, foramen for the hyomandibular branch of the facial nerve (CN VII); fo, fenestra ovalis; f.pbVII, foramen for the palatine branch of the facial nerve (CN VII); f.tfc, foramen for the trigemino-facialis chamber; f.VII, foramen for the facial nerve (CN VII); f.VIII, foramen for the acoustic nerve (CN VIII); f.XII, foramen for the hypoglossal nerve (CN XII); hsc, horizontal semicircular canal; io.f.pbVII, internal opening of the foramen for the palatine branch of the facial nerve (CN VII); io.jf, internal opening of the jugular foramen; jf, jugular foramen; jxr, juxtastapedial recess; lf, laterosphenoid foramen; ls, laterosphenoid ossification; marst, medial aperture of the recessus scalae tympani, oc, occipital condyle; otc, otic capsule; psc, posterior semicircular canal; scr, sagittal crest; sf, stapedial footplate; ss, stapedial shaft; V2, foramen for the maxillary (V2) branch of the trigeminal nerve (CN V); V3, foramen for the mandibular (V3) branch of the trigeminal nerve (CN V).

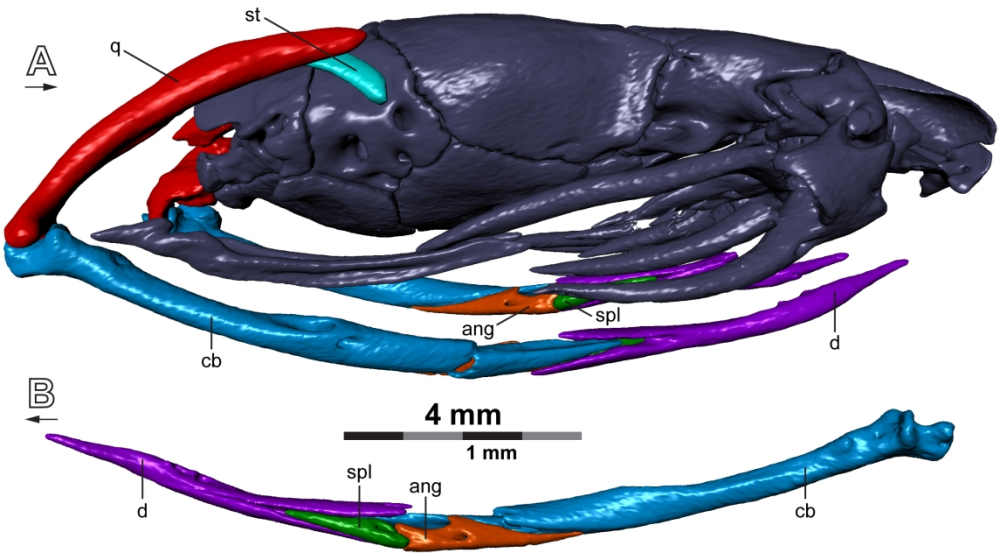

Figure 8. Suspensorium and mandible of *Atractaspis irregularis* (FMNH 62204). (A) Suspensorium and mandible in articulation with the skull (right lateral view). (B) Articulated right mandible in medial view. Colouration of bones is consistent throughout all panels. Arrows beneath panel labels point anteriorly. Surface mesh files of each element are available as 3D PDFs in the Supporting Information (Figs S1–S23). Abbreviations: ang, angular; cb, compound bone; d, dentary; q, quadrate; spl, splenial; st, supratemporal.

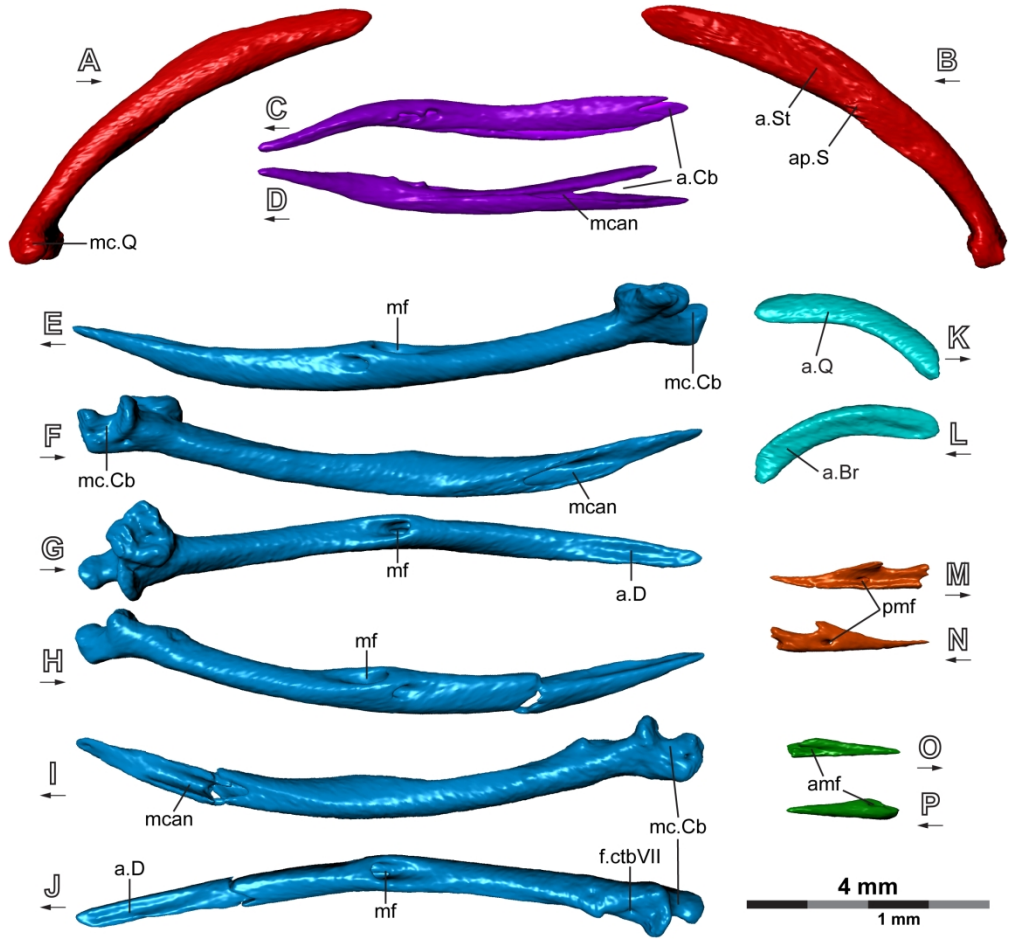

Figure 9. Suspensorial and mandibular elements of *Atractaspis irregularis* (FMNH 62204). (A–B) Right quadrate in (A) lateral and (B) medial views. (C–D) Right dentary in (C) dorsal and (D) medial views. (E–G) Left compound bone in (E) lateral, (F) medial, and (G) dorsal views. (H–J) Right compound bone in (H) lateral, (I) medial, and (J) dorsal views. (K–L) Right supratemporal in (K) lateral and (L) medial views. (M–N) Right angular in (M) lateral and (N) medial views. (O–P) Right splenial in (O) lateral and (P) medial views. Both left and right compound bones are depicted due to likely pathologic alteration posteriorly on the left counterpart and breakage anteriorly on the right counterpart. Colouration of bones is consistent with other figures. Arrows beneath panel labels point anteriorly. Surface mesh files of each element are available as 3D PDFs in the Supporting Information (Figs S1–S23). Abbreviations: a.Br, articulatory surface for the braincase; a.Cb, articulatory surface for the compound bone; a.D, articulatory surface for the dentary; amf, anterior mylohyoid foramen; ap.S, articulatory process for the stapes; a.Q, articulatory surface for the quadrate; a.St, articulatory surface for the supratemporal; f.ctbVII, foramen for the chorda tympani branch of the facial nerve (CN VII); mcan, Meckelian canal; mc.Cb, mandibular condyle of the compound bone; mc.Q, mandibular condyle of the quadrate; mf, mandibular fossa; pmf, posterior mylohyoid foramen.

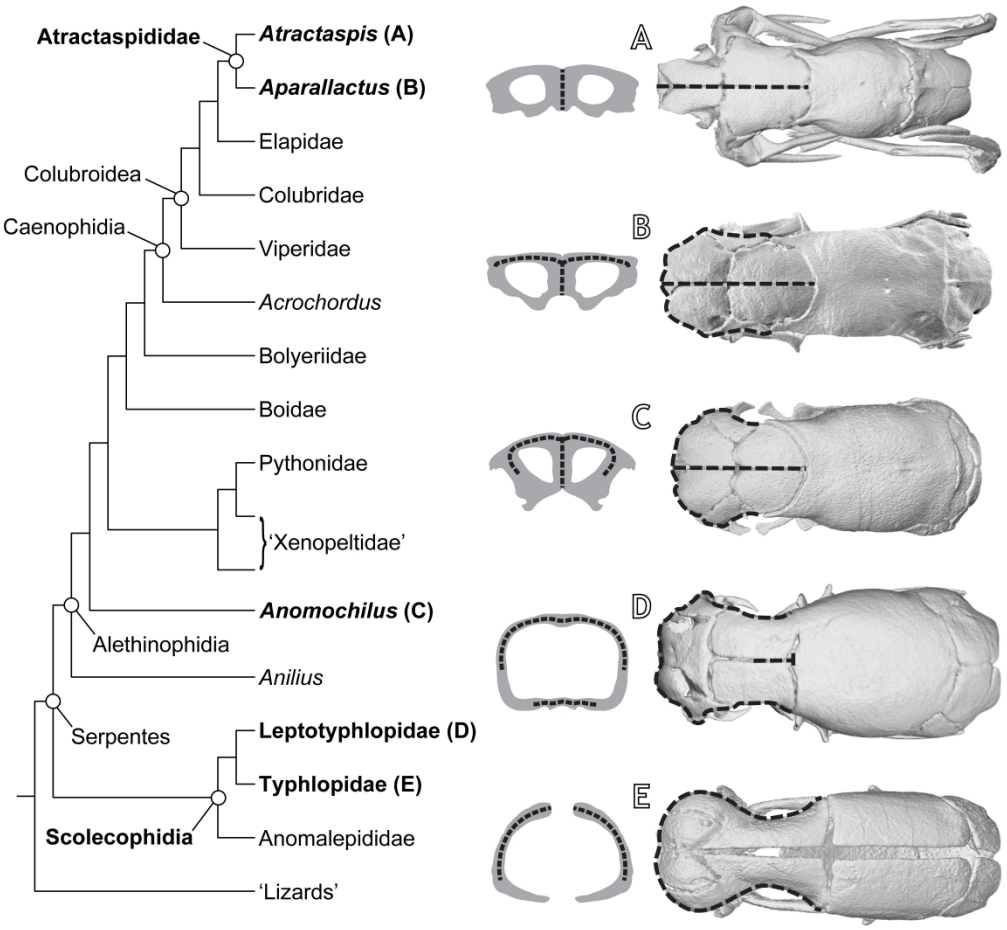

Figure 10. Morphology of the naso-frontal joint in select fossorial snakes. Each panel shows a cross-section of the frontal and a dorsal view of the skull. Dashed lines represent transmission of force while burrowing, as described by Cundall and Rossman (1993) and Rieppel et al. (2009). Key taxa are indicated in bold. (A) *Atractaspis irregularis* (FMNH 62204), exemplifying the 'central rod design' of the skull in fossorial snakes. (B) *Aparallactus werneri* (FMNH 250439), representing a mixture of the 'central rod' and 'outer shell' designs in an atractaspidid snake. (C) *Anomochilus leonardi* (FRIM 0026), representing a mixture of the 'central rod' and 'outer shell' designs in an alethinophidian snake. (D) *Leptotyphlops dulcis* (UAMZ R335), representing a mixture of the 'central rod' and 'outer shell' designs in a scolecophidian snake. (E) *Indotyphlops braminus* (UAMZ R363), exemplifying the 'outer shell design' of the skull. Phylogeny from the combined-data analysis of Hsiang et al. (2015). Specimens not to scale.

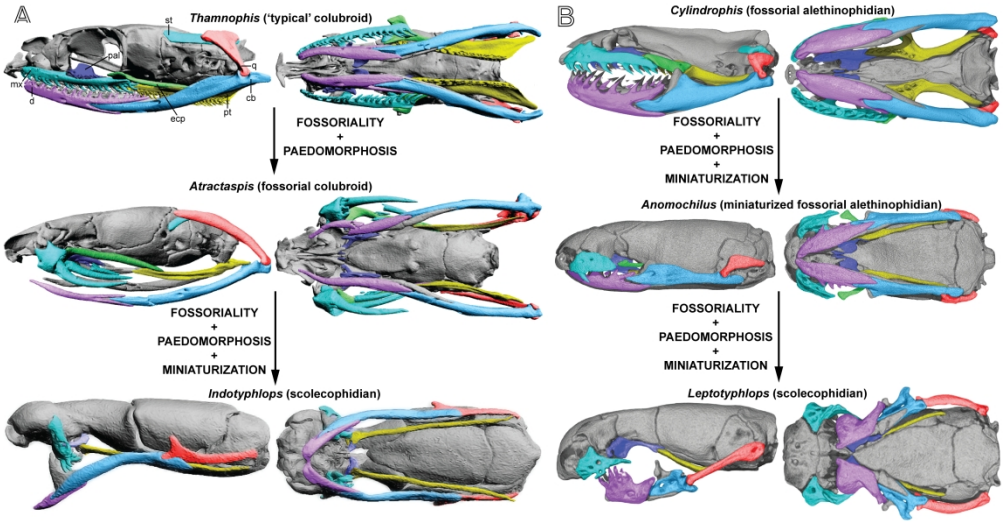

Figure 11. 'Regressed alethinophidian' hypothesis of scolecophidian evolution. (A) Example of how 'regression' from a 'typical' or non-fossorial alethinophidian skull (represented by the colubroid *Thamnophis radix*, UAMZ R636), to a fossorial alethinophidian (represented by *Atractaspis irregularis*, FMNH 62204), to a typhlopoid skull morphology (*Indotyphlops braminus*, UAMZ R363) could easily occur due to fossorial adaptations, paedomorphosis, and miniaturization. (B) Example of how the leptotyphlopid skull (*Leptotyphlops dulcis*, TNHC 60638) could easily be derived from that of a basal alethinophidian (*Cylindrophis ruffus*, FMNH 60958) through accumulation of fossorial adaptations, paedomorphosis, and miniaturization. In this scenario, *Anomochilus leonardi* (FRIM 0026) would represent an ideal morphological intermediate between the two endpoint skull types. We propose that miniaturization in scolecophidians further superimposes unique features overtop an ancestral fossorial alethinophidian morphotype. Note that these are only examples of morphological grades and do not imply phylogenetic relationships, only that the scolecophidian skull typology could be derived from an ancestral alethinophidian condition. Elements of the jaws and suspensorium affected by paedomorphosis are highlighted. Colouration of bones is consistent throughout panels. Specimens not to scale. Abbreviations: cb, compound bone; d, dentary; ecp, ectopterygoid; mx, maxilla; pal, palatine; pt, pterygoid; q, quadrate; st, supratemporal.

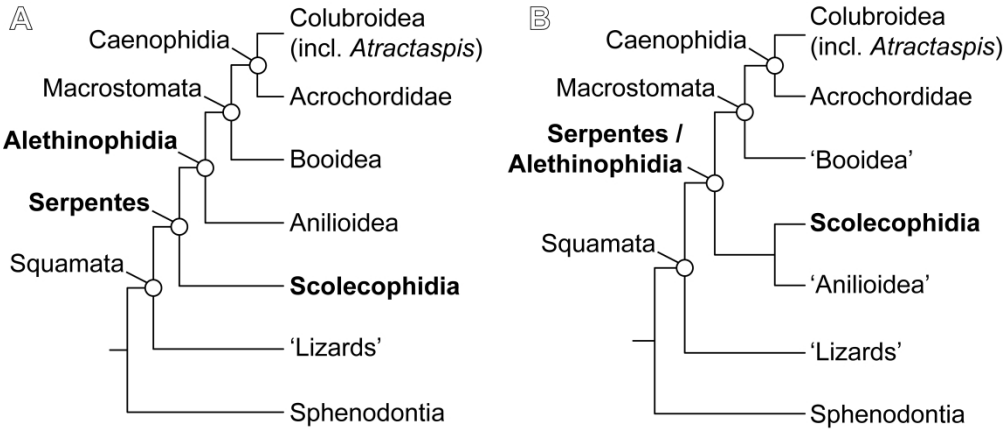

Figure 12. Competing hypotheses of scolecophidian evolution. (A) Traditional phylogeny of extant snakes (Serpentes), in which scolecophidians are the earliest-diverging lineage. (B) Recent phylogeny recovering scolecophidians as 'regressed alethinophidians', i.e., descended from an alethinophidian ancestor. Key groups are indicated in bold. Quotation marks indicate paraphyletic groups. Topologies in (A) and (B) are adapted from Rieppel (1988) and Garberoglio et al. (2019), respectively.

Insights into skull evolution in fossorial snakes, as revealed by the cranial morphology of *Atractaspis irregularis* (Serpentes: Colubroidea)

SUPPORTING INFORMATION: HRXCT Scan Parameters

(Provided by Dr. J. Maisano and DigiMorph.org)

1024x1024 16-bit TIFF images. II, 180 kV, 0.133 mA, no filter, empty container wedge, no offset, slice thickness 2 lines (= 0.0359 mm), S.O.D. 52 mm, 1600 views, 2 samples per view, inter-slice spacing 2 lines (= 0.0359 mm), field of reconstruction 15 mm (maximum field of view 17.02393 mm), reconstruction offset 6900, reconstruction scale 1400. Acquired with 15 slices per rotation. Drift- and ring-removal processing based on correction of raw sinogram data using IDL routines "RK_SinoDeDrift" with default parameters and "RK_SinoRingProcSimul" with parameter "binwidth=21". Total slices = 585.

For Peer Review Only

Insights into skull evolution in fossorial snakes, as revealed by the cranial morphology of *Atractaspis irregularis* (Serpentes: Colubroidea)

SUPPORTING INFORMATION: Pathological Elements of FMNH 62204 (*Atractaspis irregularis*)

FMNH 62204 was used as the primary reference specimen for this study, because it is openly available for visualization on DigiMorph.org. However, this specimen exhibits certain skeletal pathologies, as described below. The in-text figures display the non-pathological counterpart of the affected elements whenever possible. Other *A. irregularis* individuals (MCZ R-48555, MCZ R-49237) were also examined to ensure that the osteological descriptions in the main text represent the true conditions of each skull element.

Pterygoid

The right pterygoid has a healed fracture posteriorly, in contrast to the more uniform rod-like form of the left pterygoid. The left pterygoid was used as the basis for the description and figures in the main text.

Quadrate

The left quadrate is pathologically deformed, with the quadrate shaft broken near its mandibular condyle and the condyle itself being greatly expanded. As such, the right quadrate was used for the description and figures presented in the main text.

Compound bone

For Peer Review Only

The mandibular condyle of the left compound bone is pathologically deformed, being greatly expanded. However, this element is otherwise intact. The right compound bone is broken near its anterior terminus, though the overall morphology of the compound is otherwise intact. By combining the “normal”/non-pathological portion of the left compound bone with the “normal”/non-pathological mandibular condyle of the right compound bone, the overall morphology of this element can easily be determined and described.

Dentary

The anterior half of the left dentary exhibits 2 major breaks. The right dentary is intact, so was used as the basis for the description and figures presented in the main text.

For Peer Review Only